

Modeling river plume dynamics with the HYbrid Coordinate Ocean Model

Rafael V. Schiller*, Vassiliki H. Kourafalou

University of Miami, Rosenstiel School of Marine and Atmospheric Science, RSMAS/MPO, 4600 Rickenbacker Cswy, Miami, FL, USA

ARTICLE INFO

Article history:

Received 9 June 2008

Received in revised form 7 December 2009

Accepted 13 December 2009

Available online 21 December 2009

Keywords:

River plumes
Numerical modeling
Coastal processes
HYCOM

ABSTRACT

The dynamics of large-scale river plumes are investigated in idealized numerical experiments using the HYbrid Coordinate Ocean Model (HYCOM). The focus of this study is to address how the development and structure of a buoyant plume are affected by the outflow properties, as impacted by processes within the estuary and at the point of discharge to the coastal basin. Changes in the outflow properties involved vertical and horizontal redistribution of the river inflow and enhanced vertical mixing inside an idealized estuary. The development of the buoyant plume was evaluated in a rectangular, f -plane basin with flat and sloping bottom conditions and in the absence of other external forcing. The general behavior of a mid-latitude river plume was reproduced, with the development of a surface anticyclonic bulge off the estuary mouth and a surface along-shore coastal current which flows in the direction of Kelvin wave propagation (“downstream”); the momentum balance was predominantly geostrophic. Conditions within the estuary and the outflow properties at the river mouth (where observed profiles may be available) greatly impacted the fate of riverine waters. In flat bottom conditions, larger mixing at the freshwater source enhanced the estuarine gravitational circulation, promoting larger upward entrainment and stronger outflow velocities. Although the overall geostrophic balance was maintained, estuarine mixing led to an asymmetry of the currents reaching the river mouth and to a sharp anticyclonic veering within the estuary, resulting in reduced upstream flow and enhanced downstream coastal current. These patterns were altered when the plumes evolved in the presence of a bottom slope. The anticyclonic veering of the buoyant outflow was suppressed, the offshore intrusion decreased and the recirculating bulge was displaced upstream. The sloping bottom impacts were accompanied by enhanced transport and increased downstream extent of the coastal current in most cases. No major changes in the general properties and especially the vertical structure of the plumes were observed when the vertical coordinates were changed from cartesian–isopycnal, to sigma or to sigma–isopycnal. The findings offer a benchmark for coastal studies with HYCOM, where plume dynamics should be examined in tandem with additional circulation forcing mechanisms, resulting in transitions of the vertical coordinate system that are dictated by the prevailing dynamics.

© 2009 Elsevier Ltd. All rights reserved.

1. Introduction

The dynamics of large-scale river outflows (affected by the earth’s rotation) have been widely investigated in the literature. It is acknowledged that in the absence of external forcing (such as winds, tides, and ambient currents) and if a river buoyant plume is large enough to be affected by the Coriolis force, riverine waters will turn anticyclonically when they reach the shelf, and move away from their land source as an along-shore buoyancy driven coastal current, in the direction of Kelvin wave propagation (hereafter referred to as “downstream direction”). Observations of large river plumes on open shelves such as along the US east and west coasts include: the Delaware (Münchow and Garvine, 1993a,b)

and the Chesapeake (Boicourt, 1973; Marmorino and Trump, 2000) Bays, the Columbia (Hickey et al., 1998, 2005; Horner-Devine, 2009), the Hudson (Chant et al., 2008) and the Niagara (Masse and Murthy, 1992; Horner-Devine et al., 2008) Rivers, and the low salinity coastal band in the South Atlantic Bight (Blanton et al., 1994). Satellite and field studies have also shown evidence of a bulge-like region in the vicinity of the river inflow, where plume waters recirculate before feeding the coastal current (Masse and Murthy, 1992; Hickey et al., 1998; Chant et al., 2008; Horner-Devine et al., 2008; Horner-Devine, 2009). Similar behavior has also been observed in laboratory studies (Stern et al., 1982; Griffiths and Hopfinger, 1983; Whitehead and Chapman, 1986; Avicola and Huq, 2003a,b; Horner-Devine et al., 2006).

In addition to observations, numerical and analytical models have been used to understand and clarify the dynamics of coastal buoyant plumes. Many studies have been conducted in idealized scenarios. Rectangular basins were employed with simplified

* Corresponding author. Tel.: +1 305 421 4654; fax: +1 305 421 4696.

E-mail addresses: rschiller@rsmas.miami.edu (R.V. Schiller), vkourafalou@rsmas.miami.edu (V.H. Kourafalou).

bottom topography, with buoyancy forcing only or with additional simple external forcing, such as constant and unidirectional winds, along-shore ambient current and single component tides. Such idealized studies revealed many features of river plume dynamics generally hard to extract from observations, where complex circulation forcing mechanisms impact the plume behavior. Early studies recognized the importance of non-linearity, rotation and friction in the development of the frontal structure of large buoyant discharges (Kao et al., 1977; Kao, 1981; Ikeda, 1984; Garvine, 1987). Pioneering numerical modeling studies demonstrated the impact of vertical mixing, bottom drag and sloping bottom on the spin-up, maintenance and dissipation of river-forced plumes (Chao and Boicourt, 1986; Chao, 1988a,b) as well as the coastal current variability associated with barotropic and baroclinic instabilities (Oey and Mellor, 1993). The variability of the bulge and the coastal current from a river-forced plume was also demonstrated by Kourafalou et al. (1996), who elucidated the effects of buoyancy-induced stratification versus available mixing in determining the expansion of the bulge and the coastal current meandering.

The importance of the river mouth conditions to the variability of the bulge and coastal current transport has been reported by several studies. Yankovsky and Chapman (1997) developed a theory which relates properties of the estuarine discharge and cross-shore bottom slope to the bulge and coastal current structure. Garvine (1999) verified that the estuarine volume transport, scaled by the associated outflow geostrophic transport, controlled the greatest variance of the downshelf and across-shelf plume penetration. Fong and Geyer (2002) demonstrated that river mouth conditions affect the amount of freshwater transported by the coastal current relative to the bulge, which can accumulate low salinity waters, become unsteady and grow in time. They observed that when river outflows with larger Rossby number were simulated, more plume water recirculated within the bulge and that decreased the coastal current freshwater transport. In a series of laboratory experiments, Avicola and Huq (2003a,b) demonstrated how the “outflow angle” (angle between the outflow and the coastal wall) and the “impact angle” (angle at which the buoyant flow reattaches to the coast) affect the formation of the recirculating bulge. They suggested that the two angles are related (the outflow angle determines the impact angle) and concluded that a coastal current formed at oblique impact angles, and the bulge recirculation increased as the impact angle approached 90°. Finally, Yankovsky (2000) and Garvine (2001) demonstrated that the implementation of the river boundary conditions may affect the near-field bulge circulation, more specifically the development of the plume upstream intrusion. Kourafalou et al. (1996) showed that the upstream intrusion was due to a non-geostrophic balance between the along-shore acceleration and the along-shore pressure gradient (due to low salinity waters near the river mouth and denser ambient waters up the coast). Yankovsky (2000) suggested that the upstream intrusion is enhanced by over simplified river boundary conditions that lack a baroclinic adjustment of the discharge (i.e., fixed uniform river inflow along the coastal wall). The blocking of the lower layer landward flow at the mouth promotes a strong cyclonic vorticity disturbance with corresponding upstream turning of the buoyant flow at the source, which enhances the upstream spreading of the plume. Yankovsky (2000) and Garvine (2001) concluded that the use of an inlet flow field that better mimics that observed at the mouth of estuaries (upper seaward buoyant flow on top of a lower landward undercurrent) reduces that impact.

In the study presented herein, a ocean general circulation model is employed in an idealized estuary-coastal basin system to examine the development and evolution of a river plume under buoyancy forcing only and to investigate the plume variability associated with changes in the conditions at the river mouth. These changes are shown to be the results of lateral and vertical spread-

ing of the river inflow and variable mixing inside the estuary. These effects are expected to impact the estuarine circulation and the buoyant outflow, ultimately promoting changes in the recirculating bulge and the coastal current properties. Previous numerical modeling studies (Chao and Boicourt, 1986; Chao, 1988a; MacCready et al., 2009) have demonstrated the importance of the estuarine circulation to the development of the river plume. The focus of the study presented herein is to understand how the properties of the buoyant flow at the estuary mouth (which reflects the coupling between the estuarine and basin circulations) impact the development of the river plume in the receiving basin.

We employ the HYbrid Coordinate Ocean Model (HYCOM; Bleck, 2002; Halliwell, 2004; Chassignet et al., 2006), which is used for the first time to investigate the dynamics of river plumes and the offshore propagation of buoyant waters. HYCOM is a state of the art community model that has been designed as a finite-difference and hybrid isopycnal–sigma–cartesian vertical coordinate ocean model with the objective to provide a flexible vertical coordinate system that is quasi-optimal in all oceanic regimes. Although initially applied on large scale, open ocean processes, the philosophy behind the flexibility in the vertical coordinate system was based on the desire to fully address coastal to offshore interactions. Our methodology includes the use of innovative parameterizations within the HYCOM code which comprise: a river parameterization option that allows enhanced downward penetration of the buoyant input and/or enhanced lateral spreading of riverine waters; adoption of different vertical mixing schemes; changes in basin topography and in the choice of vertical coordinates. This paper is organized as follows: Section 2 gives a brief description of HYCOM, the model capabilities and parameterizations for this study. Section 3 provides a description of the domain where numerical experiments are performed. Results from flat bottom and sloping bottom basins are presented in Section 4 and are followed by a discussion in Section 5. Section 6 provides a summary of the results and conclusions.

2. Model description

HYCOM is a primitive equation ocean general circulation model supported by code development and operational global/regional simulations associated with the HYCOM Consortium for Data Assimilative Modeling (see technical details in the model manual at www.hycom.org). HYCOM has been used in several large scale and marginal seas studies (Chassignet et al., 2003; Halliwell et al., 2003; Shaji et al., 2005; Kara et al., 2005; Hogan and Hurlburt, 2006; Zamudio and Hogan, 2008), and it has been recently applied to the coastal ocean as well (Kourafalou et al., 2006, 2009; Olascoaga et al., 2006; Halliwell et al., 2009). A comprehensive discussion of HYCOM’s governing equations and numerical algorithms (including the hybrid coordinate grid generator) and the available vertical mixing schemes can be found in Bleck (2002) and Halliwell (2004). Here, HYCOM is briefly presented, with emphasis on the model aspects that are relevant for this study.

HYCOM is a finite-difference hydrostatic, Boussinesq primitive-equation model that solves 5 prognostic equations: one for each horizontal velocity component, a layer thickness tendency (mass continuity) equation, and two conservation equations for a pair of thermodynamic variables (salt, temperature or density). Here, salt and density are employed. Variables are stored on the Arakawa C grid. Thermodynamic variables and the horizontal velocity field are treated as “layer” variables that are vertically constant within layers but change discontinuously across layer interfaces. Other variables, such as pressure, are treated as “level” variables, defined on interfaces. These prognostic equations are complemented by a

hydrostatic equation, an equation of state and an equation for the vertical mass flux through the layer interfaces, which controls their vertical movement and together with the hybrid coordinate grid generator defines the layer state (cartesian, sigma or isopycnal).

The prognostic equations are time-integrated using the split-explicit treatment of barotropic and baroclinic modes presented in Bleck and Smith (1990) with modifications by Morel et al. (2008). The baroclinic part of the solution is advanced in time with a leapfrog scheme, while the traditional forward-backward scheme for the barotropic solution presented in Bleck and Smith (1990) has been replaced by a new LSBM (Leapfrog for the Slow part of the Barotropic Mode) which leads to better stability properties (Morel et al., 2008). Horizontal mass fluxes are handled using the Flux Corrected Transport (FCT) scheme (Zalesak, 1979), while horizontal tracer advection is computed using a centered difference scheme for tracer modified by an FCT procedure. Horizontal tracer diffusion and horizontal momentum viscosity follow Bleck et al. (1992). Wind-induced stress is assumed to be zero at the bottom of the mixed layer, and a quadratic form of bottom drag is employed to determine dissipation by the bottom. Different choices of vertical mixing schemes are available, which can calculate either vertical mixing throughout the water column or calculate mixed layer entrainment/detrainment separately from the weak, interior diapycnal mixing (Halliwell, 2004). Surface heat fluxes are parameterized according to Kara et al. (2000).

2.1. Freshwater flux and river inflow parameterization

In HYCOM, freshwater flux is parameterized as a virtual salt flux (Huang, 1993). While calculating vertical mixing at every baroclinic time step dt_{bcclin} , the salinity S in model layer 1 is updated to take into account changes due to freshening from river inflow or rain: $S = S + dS$. The salinity increment dS is proportional to the virtual salt flux S_f : $dS = S_f \times dt_{bcclin} \times g \times 1/dp$ and $S_f = [-(P - E) - R] \times S \times 1/\alpha_0$; g is gravity (9.806 m s^{-2}); dp is the layer thickness (in pressure units); S_f is the virtual salt flux per unit of horizontal area divided by the reference specific volume α_0 ($10^{-3} \text{ m}^3 \text{ kg}^{-1}$); P , E and R represent the precipitation, evaporation and river input contributions, respectively (translated to m s^{-1}). If freshwater is to be added, $E < P + R$, $S_f < 0$ and the salinity decreases. If freshwater is to be removed, $E > P + R$, $S_f > 0$ and the salinity increases.

This implementation does not take into account the mass of freshwater that is introduced/removed, but only the resulting density changes. In this study, the parameterization of the actual river mass inflow has been introduced by including an additional term in the barotropic pressure calculations. During the vertical mixing calculations at every baroclinic time step and at the grid points where the river inflow is imposed, the “barotropic pressure” term ($p_b \eta$) (see Bleck and Smith, 1990) is updated as $p_b \eta = p_b \eta + (dt_{bcclin} \times g \times Q_{river})/(\alpha_0 \times A_{grid})$, where Q_{river} is the freshwater flux ($\text{m}^3 \text{ s}^{-1}$) and A_{grid} is the horizontal grid area (m^2). This new formulation takes into account the pressure exerted by the mass of freshwater that is “virtually” introduced via the river inflow, and adds that contribution to the barotropic pressure of the water column. In theory, a river discharging freshwater into a more saline environment will generate a baroclinic anomaly (due to the density change) and a barotropic anomaly (due to the freshwater volume). Moreover, momentum is introduced into the system by the river inflow itself, at the head of the estuary. Although the freshwater volume anomaly is not taken into account in HYCOM, the barotropic pressure ($p_b \eta$) exerted by this anomaly is calculated. Thus estuarine momentum naturally develops via the baroclinic and barotropic circulation induced by the freshwater inflow. The lack of river inflow momentum at the head of the estuary should not be detrimental to our model results. In the current domain configuration (Section 3), a river volume inflow of 1000

$\text{m}^3 \text{ s}^{-1}$ across the estuarine area ($3 \times 10^5 \text{ m}^2$) would generate velocities of 0.003 m s^{-1} , which are much smaller than the velocities that develop inside the estuary (reaching 0.2 m s^{-1} , see Section 4).

In the original HYCOM code, the freshwater flux due to river inflow was treated similarly to precipitation, injected in the first model layer. This could cause problems if the model layers are too thin at river grid points, leading to a low salinity spike if the freshwater discharge is too high or if the model mixing is unable to mix the freshwater vertically or horizontally. Moreover, in nature, riverine waters occupy an upper layer of finite depth that changes under variable discharge and is also influenced by the available mixing conditions. An updated parameterization of river inflow in HYCOM was motivated by the present study and the user options described below (as well as the river mass inflow option discussed above) are available in the latest HYCOM code releases (Wallcraft, personal communication). The user is thus given the option to increase the downward penetration of the river inflow, effectively mixing the freshwater down to a specific depth. Another option is to increase the lateral spreading of the river inflow over specified cells. These are two ways of reducing the low salinity spike that may be created when all river discharge is concentrated in a few grid points. The physical meaning of the above modifications is to allow for additional vertical and horizontal mixing that would normally be available in realistic forcing experiments, where buoyancy is not the only external forcing.

2.2. Vertical mixing schemes

A detailed description of the vertical mixing schemes present in HYCOM is available in Halliwell (2004); an evaluation of their performances in low-resolution climatological simulations of the Atlantic Ocean is also given. In this study the three “continuous” differential models (which govern vertical mixing throughout the water column, not only at the mixing layer) are employed, namely the K-Profile Parameterization (KPP, Large et al., 1994), the NASA Goddard Institute for Space Studies level 2 turbulence closure (GISS, Canuto et al., 2001, 2002) and the Mellor–Yamada level 2.5 turbulence closure (MY2.5, Mellor and Yamada, 1982).

2.3. Hybrid vertical coordinate grid generator

The foundation of the hybrid vertical coordinate system is the work by Bleck and Boudra (1981) and Bleck and Benjamin (1993). Each vertical layer in HYCOM is assigned a target density. At the end of each baroclinic time step, the model checks the calculated layer density against its target value and, if they differ, it tries to restore the former to the latter by allowing vertical movement of layer interfaces and vertical mass fluxes between them. However, if the vertical migration of grid points creates a crowding of coordinate surfaces, the model will produce (on a chosen number of upper n_{hyb} layers) a smooth transition from the isopycnal to the cartesian, fixed domain. This crowding is evaluated through a minimum thickness enforcement specified by the user, using a “cushion” function defined in Bleck (2002). Layers that transit to cartesian levels are then allowed to change their density freely and are no longer isopycnal. Likewise, the transition to sigma levels occurs only in the same n_{hyb} layers, where again a minimum thickness condition is evaluated. The choices of coordinate separation constrains that control the transition among the coordinate choices is left to the user. That allows different vertical coordinate possibilities, such as isopycnal–cartesian, isopycnal–sigma or fully hybrid domains. The model can also be run in purely isopycnal, cartesian or sigma mode. This flexibility was explored by Chassignet et al. (2003) in North Atlantic basin experiments, and will be also explored in the experiments presented herein.

3. Box model domain set-up

Following the idealized approach of the previously mentioned river plume studies, a box-like domain has been designed. It consists of a mid-latitude, f -plane (Coriolis parameter $f = 10^{-4} \text{ s}^{-1}$) rectangular basin that is approximately 200 km long in the across-shore direction and 500 km long in the along-shore direction. The west boundary of the basin is a closed wall, whereas the north, east and south lateral boundaries are open water points. A 20 km long, 15 km wide simplified estuarine channel is located at the coast (Fig. 1). The horizontal grid spacing is 2.5 km by 2.5 km throughout the domain. The basin water is initially homogeneous, with salinity of 35 and temperature of 28 °C, and it is in a state of rest. At the head of the estuarine channel, a freshwater discharge of $1000 \text{ m}^3 \text{ s}^{-1}$ is imposed (zero salinity, temperature 28 °C). The flow field is left to evolve for a period of 60 days. At the offshore lateral open boundaries, the baroclinic structure of the flow is relaxed to the basin initial state, whereas the barotropic structure is solved through the method of characteristics (Brown and Kreiss, 1982, 1986). At the closed lateral boundary (the coast), a no-slip condition is applied to parallel velocities, and normal velocities are set to zero. At the bottom, momentum is dissipated by a quadratic bottom drag (drag coefficient $C_d = 3 \times 10^{-3}$), using a bottom velocity u_b that represents the average velocity in a slice of water situated just above the bottom. If the KPP vertical mixing scheme is used, this thickness is determined by a bottom boundary layer parameterization that is an adaptation of the algorithm used for the surface boundary layer (Halliwell et al., 2009). Otherwise, it is set to 1 m. Salt flux normal to the bottom and the coast is zero. At the surface, the river precipitation bogus is the only forcing mechanism.

Flat and sloping bottom topography configurations are employed. In the flat bottom set-up, 16 cartesian levels are used in the vertical and the bottom is 20 m deep everywhere (layer spacing is 1.25 m), which is a reasonable approximation to average inner-shelf depths. In the sloping bottom set-up, a gentle slope starts at the coast line. The estuary remains 20 m deep and the shelf bottom depth goes down to 100 m within 200 km in the offshore direction. Now, a temperature profile is imposed such that the temperature is 28 °C at the surface and decreases 0.5 °C every

5 m. The presence of a sloping bottom and ambient stratification allow the use of a fully hybrid vertical level set-up in this domain. The standard configuration for sloping bottom experiments is 24 fixed cartesian levels in the upper 30 m (layer spacing is 1.25 m) and 6 isopycnal levels from 30 m to 100 m (Fig. 1). This configuration enforces vertical resolution in the upper water column to be the same as in the flat bottom experiments, and avoids the interaction of deep isopycnal levels with the surface plume dynamics while taking the advantage of the flexible vertical coordinate system in HYCOM. Sloping model experiments with all sigma layers (30 terrain following layers) and with a combination of sigma in the upper 50 m and isopycnal below, were also employed.

4. River plume experiments

A series of experiments were employed for both the flat and sloping bottom basin configurations described in Section 3. Twelve combinations of model parameters were explored, see attributes in Table 1.

4.1. Control experiment

A control experiment is configured to serve as “reference” against other experiments, as well as to evaluate the general plume dynamics. It employs the basic HYCOM river parameterization (precipitation bogus, no downward penetration, no lateral spreading) with mass inflow parameterization included. Vertical mixing is governed by the KPP scheme.

The development of the control buoyant plume in the 20 m deep, flat bottom basin (Control-flat) follows the general description in the literature (Chao and Boicourt, 1986; Chao, 1988a; Kourafalou et al., 1996; Garvine, 1999, among others). The buoyant plume reaches the shelf by day 5, while making an anticyclonic turn at the mouth of the estuary (not shown). A recirculating bulge develops and grows in time, followed by a coastal current propagating in the downstream direction. The river plume is well developed after 60 days (Fig. 2), with a coastal current ($\sim 6\text{--}8 \text{ cm s}^{-1}$) that presents a developed meandering character due to barotropic/baroclinic instabilities (Oey and Mellor, 1993). An upstream penetration is also observed. Taking the plume boundary to be

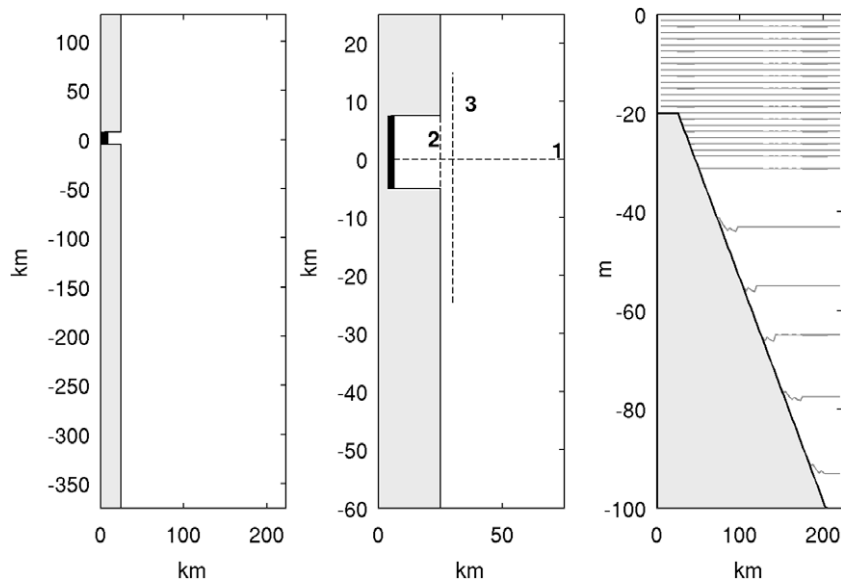


Fig. 1. Model configuration. (Left) Idealized box-like basin. The thick short black line denotes where river discharge is imposed (estuary head). Land area is shaded. (Center) Zoom of the estuarine region. Dashed lines show positions of vertical sections where model results are evaluated: along the estuary and across the basin (1), across the estuary mouth (2) and along-shore in the vicinity of the estuary (3). (Right) Vertical section of bathymetry from the sloping bottom set-up showing vertical levels (thin lines, along Section 1); additional hybrid configurations are exhibited in Fig. 13.

Table 1

Summary of the attributes from the study experiments. Downward penetration is given in percentage of the water column and in meters (parentheses). Lateral spreading is classified as none, short (4 grid points, half-estuary length) or large (7 grid points, full-estuary length). KPP background vertical mixing is characterized as standard (no modifications) or as Enhanced K_{iw} (salinity diffusivity due to background internal wave mixing equals $10^{-4} \text{ m}^2 \text{ s}^{-1}$) plus region where it is applied. See Sections 4.2 and 4.3 for details.

Experiment	Downward penetration (pntr)	Lateral spreading (sprd)	KPP background vertical mixing
Control	0% (0)	None	Standard
Riv1b	20% (4)	None	Standard
Riv1c	40% (8)	None	Standard
Riv2a	0% (0)	Short	Standard
Riv2b	20% (4)	Short	Standard
Riv2c	40% (8)	Short	Standard
Riv3a	0% (0)	Large	Standard
Riv3b	20% (4)	Large	Standard
Riv3c	40% (8)	Large	Standard
Mix4a	0% (0)	None	Enhanced K_{iw} at the estuary head
Mix4b	0% (0)	None	Enhanced K_{iw} over half-estuary length
Mix4c	0% (0)	None	Enhanced K_{iw} over full-estuary length

the 34.9 salinity isoline, the nose of the coastal current has reached 202.5 km south of the river mouth. The offshore extension of the bulge (72.5 km) is larger than the coastal current width (62.5 km), which represents a supercritical plume case (Chao, 1988a). A weaker undercurrent (not shown) runs in the upstream direction opposite to the downstream coastal current below 6–8 m, with velocities around 3 cm s^{-1} . An across-shore vertical section of salinity contours (Fig. 2) shows that the buoyant flow forms a 2-layer structure, with a surface buoyant layer on top of denser ambient water. This is the case of a surface-advected plume (Yankovsky and Chapman, 1997), which presents a recirculating bulge, a coastal current close to the coast and very little contact with the bottom. The maximum barotropic velocity at the bulge reaches 3 cm s^{-1} , well below the maximum baroclinic velocity (12 cm s^{-1}).

In sloping bottom conditions (Control-slope, Fig. 3), the plume develops a recirculating bulge that is elongated in the upstream direction and shortened in the offshore direction in comparison to

Control-flat. An enhanced upstream intrusion develops, as most of the buoyant outflow turns to the left upon exiting the estuary, before turning anticyclonically and merging to the coastal current (which exhibits less meandering). The enhancement of the upstream and shortening of the offshore intrusions have been reported in previous studies (Kourafalou et al., 1996; Garvine, 1999), and the changes in the bulge structure suggest the effect of potential vorticity constraints imposed by the bottom slope (Chao, 1988a).

4.2. Prescribed river inflow distributions inside the estuary

We examine changes in the development and structure of the river plume when the river inflow distribution is prescribed inside the estuary. This is accomplished by employing the river parameterization options of enhanced downward penetration and horizontal spreading of the river inflow (described in Section 2.1), which effectively change the vertical and horizontal mixing of the buoyant plume at the source. This redistribution of freshwater input is expected to change the properties of the buoyant outflow at the estuary mouth and impact the development of the river plume in the receiving basin. We enhance the downward penetration of the river inflow to 20% (4 m) and 40% (8 m) of the water column and impose a short lateral spreading (half the estuary length) and a large lateral spreading (the entire estuary length). Together with the Control case, nine different parameter combinations for the study experiments are employed (Table 1); “experiment(s)” will be abbreviated “expt(s)” thereafter. All expts in this group employ the KPP vertical mixing scheme. Snapshots of the plume Sea Surface Salinity (SSS) and the bulge near surface velocity vectors (both at day 60) are presented in Figs. 4 and 5, respectively. The extensions of each plume upstream (L_u), downstream (L_d) and offshore (L_o) intrusions are also depicted in Fig. 4.

4.2.1. Variable downward penetration and no lateral spreading

Cases of variable downward penetration (0%, 20% and 40%) with no lateral spreading of the river inflow are shown in Fig. 4 (upper panels). There is a considerable change in the shape and extension of the plume when the downward penetration of the river discharge is enhanced to 20% (expt Riv1b-flat); the anticyclonic bulge grows in size, with a larger offshore extension and a more circular

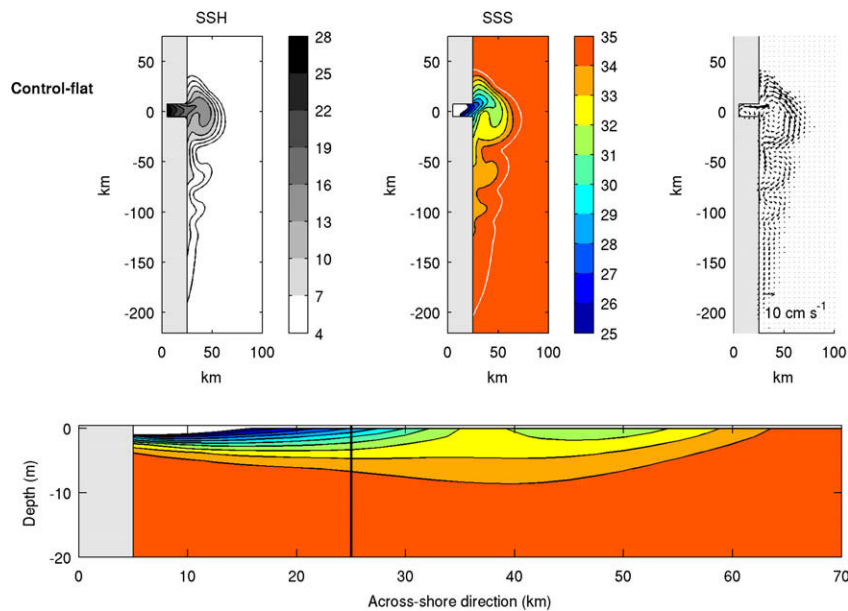


Fig. 2. (Upper) Sea Surface Height contours in mm (SSH, left), Sea Surface Salinity contours (SSS, middle) and near surface velocity vectors in cm s^{-1} (right) from the Control-flat experiment at day 60 (part of the model domain shown). (Lower) Along-estuary/across-shore salinity vertical structure along Section 1 (marked in Fig. 1). The plume boundary (34.9) is represented by a white line. Salinity values less than 25 (inside the estuary) are not shown. Vertical black line denotes the position of the estuary mouth.

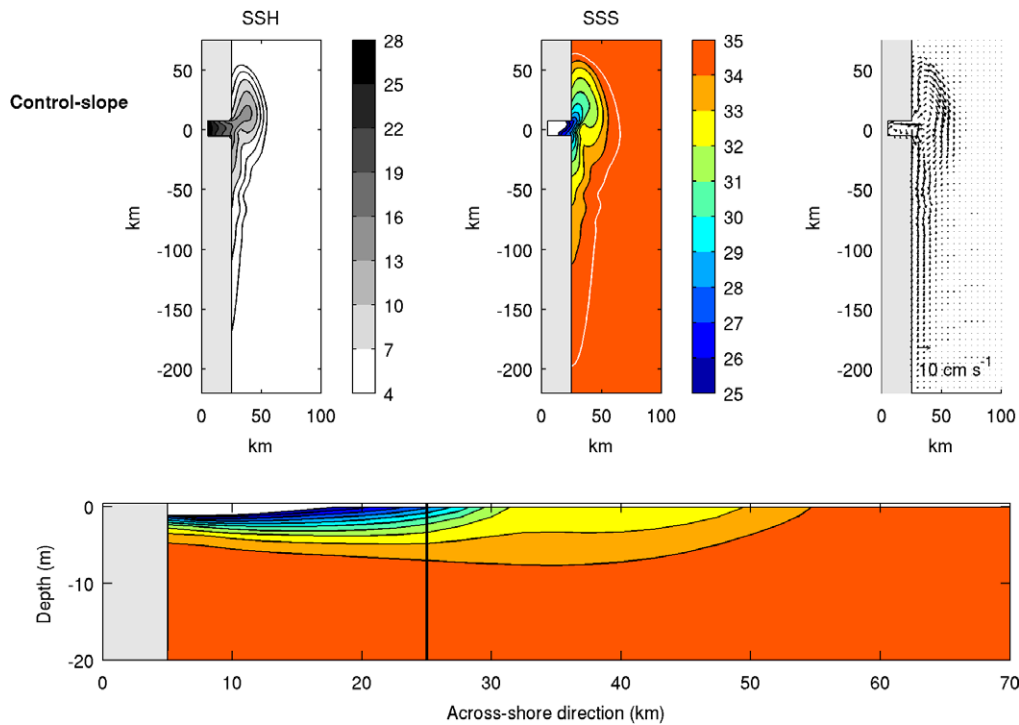


Fig. 3. As Fig. 2, but for the Control-slope experiment.

shape. A stronger coastal current is present, with more meanders and a longer downstream extension. Interestingly, the upstream penetration is much reduced. This pattern is enhanced when this mixing is forced down to 40% of the water column (Riv1c-flat). In all cases, the buoyant outflow is denser with increasing downward penetration of the inflowing river discharge. The surface circulation from these experiments (Fig. 5, upper panels) demonstrates a progressive strengthening of the buoyant outflow with increasing downward penetration of the river inflow by 20% (Riv1b-flat) and 40% (Riv1c-flat). A shift in the position and direction of the estuary outflow is also observed, which has clear impact on the shape and location of the offshore bulge. The plume outflow is concentrated in the northern wall of the estuary mouth and exits in a straight path (Control-flat), and as it intensifies it spreads across the estuary mouth (Riv1b-flat) and develops an enhanced anticyclonic turning (Riv1c-flat).

The effect of the bottom slope is demonstrated on the Riv1c case, depicting a marked impact on both the estuary outflow and the bulge development (Riv1c-slope, Figs. 4 and 5). In this case the buoyant outflow does not present an anticyclonic veering, as it exits the estuary in a straight path (similar to Control-slope). The bulge presents a marked upstream displacement and upstream flow intrusion, which are accompanied by a shorter offshore extent. As the bottom slope “squeezes” the buoyant flow area against the coast, the plume is elongated in the along-shore direction and develops a longer coastal current region.

4.2.2. Variable downward penetration and short lateral spreading

The general pattern in the surface salinity field discussed above (reduction of the upstream intrusion, larger offshore bulge and larger downstream penetration) is also observed when the downward penetration of the river inflow is increased in the presence of short lateral spreading (Fig. 4, middle panels). However, some distinctions from the same cases with no lateral spreading are observed. The upstream intrusion enhances from the expt Control-flat to Riv2a-flat and the bulge is slightly less circular in expt

Riv2b-flat than in Riv1b-flat. No major changes are observed in the salinity field from expts Riv1c-flat and Riv2c-flat, except the outflow from Riv2c-flat is less buoyant and the bulge is larger than in experiment Riv1c-flat. The general pattern of buoyant outflow intensification and development of an anticyclonic veering is also observed when downward penetration increases from 0 to 40% (Fig. 5, middle panels). Finally, the trend imposed by the bottom slope in expt Riv1c-slope is also observed in Riv2c-slope, where the bulge is displaced in the upstream direction, the outflow does not develop an anticyclonic veering and the coastal current region is elongated.

4.2.3. Variable downward penetration and large lateral spreading

The plume surface salinity field changed considerably when the vertical penetration of the river inflow was varied while employing large spreading (Figs. 4 and 5, lower panels), as now both vertical and horizontal salinity gradients were impacted. The same pattern of enhancement of the upstream intrusion is observed at 0% downward penetration (Riv3a-flat), which vanishes at 20% downward penetration (Riv3b-flat) as the bulge becomes less circular and less distinct from the coastal current (in comparison to Riv2b-flat). The largest changes in plume shape were observed at 40% downward penetration (Riv3c-flat), when the offshore bulge did not develop and the plume turned abruptly to the right and moved downstream forming a coastal current that started unidirectional and then developed a meandering pattern, starting with a feature resembling a secondary bulge due to the large amount of low salinity water that has leaked along the coast. The near surface velocity field (Fig. 5, lower panels) confirms that the outflow from expt Riv3c-flat developed an abrupt right turn at the estuary mouth and all plume waters were deflected southward, increasing the downstream coastal current penetration. Conversely, the development of the plume in sloping bottom conditions (Riv3c-slope) is considerably different as an offshore bulge develops in front of the estuary, the buoyant outflow exits in a straight path and a slight upstream intrusion is observed. The presence of a slope ap-

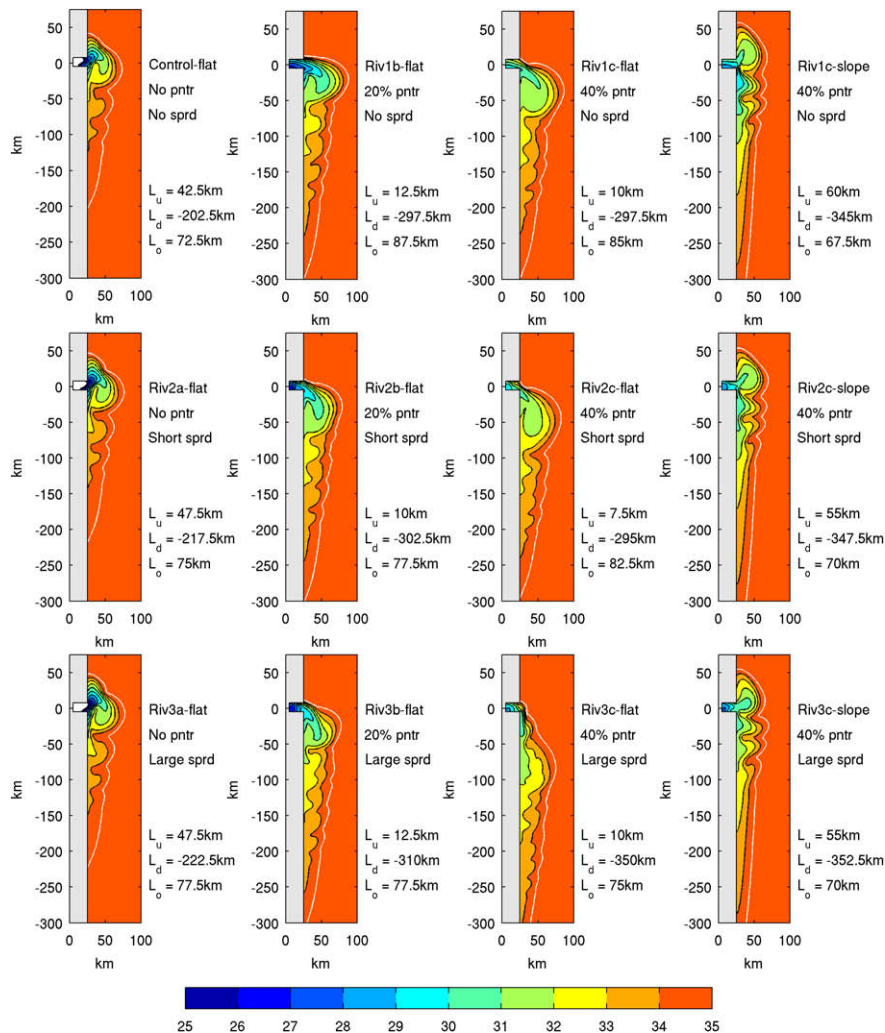


Fig. 4. Sea Surface Salinity contours from experiments with variable distribution of river inflow inside the estuary, at day 60 (part of the model domain shown). The plume boundary (34.9) is represented by a white line. Salinity values less than 25 (inside the estuary) are not shown. The upstream (L_u), downstream (L_d) and offshore (L_o) plume intrusions for each case are displayed next to the plots. Downward penetration (pntr) and horizontal spreading (sprd) configurations that characterize each experiment are also presented.

pears to overwhelm the impact of lateral and/or vertical mixing inside the estuary, as suggested by the similarities of the Riv2c–slope and Riv3c–slope expts, in contrast to their clearly different flat bottom counterparts.

4.3. Enhanced vertical mixing inside the estuary

The impact of changes in the vertical mixing at the freshwater source on the development of the river plume is also investigated. Instead of mixing the river freshwater by redistributing it, the background mixing within the KPP vertical mixing scheme was enhanced. Specifically, the vertical salinity diffusivity due to background internal wave mixing K_{iw} was increased to $10^{-4} \text{ m}^2 \text{ s}^{-1}$ (10 times its standard background value) inside the estuary. Three expts were performed, where K_{iw} was enhanced in three distinct regions: at the estuary head, from the head to half the estuary length and from the head to the estuary mouth (full-estuary length). The choice to change K_{iw} and not other aspects of the KPP vertical mixing scheme was based on the fact that the background internal wave mixing is the main contributor to vertical mixing in the study experiments (see discussion below). In order to access the sensitivity of the plume structure to the choice of

vertical mixing scheme, twin expts of the Control–flat case that employ the MY2.5 and GISS vertical mixing schemes were performed.

The enhancement of K_{iw} inside the estuary effectively impacts the outflow properties and the development of the buoyant plume. SSS and near surface velocity vectors from this group of experiments (Fig. 6) demonstrate that as the estuarine region was mixed through enhanced K_{iw} , the outflow became less fresh, progressively developed an anticyclonic turning and decreased the plume upstream penetration. The offshore bulge was clearly impacted by those changes, as it is shown to shift downstream and finally vanish with the outflow being deflected in the downstream direction. The surface fields from the half-estuary (Mix4b–flat) and full-estuary (Mix4c–flat) cases resemble those impacted by 40% downward penetration at short (Riv2c–flat) and large (Riv3c–flat) horizontal spreading, respectively. In the presence of the bottom slope (Mix4c–slope), the plume evolves to the same structure as in the expt Riv3c–slope.

The mixing expts revealed that the plume structure was not sensitive to the choice of vertical mixing schemes. Employing the MY2.5 or the GISS vertical mixing schemes produced river plumes that had the same vertical salinity structure as the Control experiment (KPP),

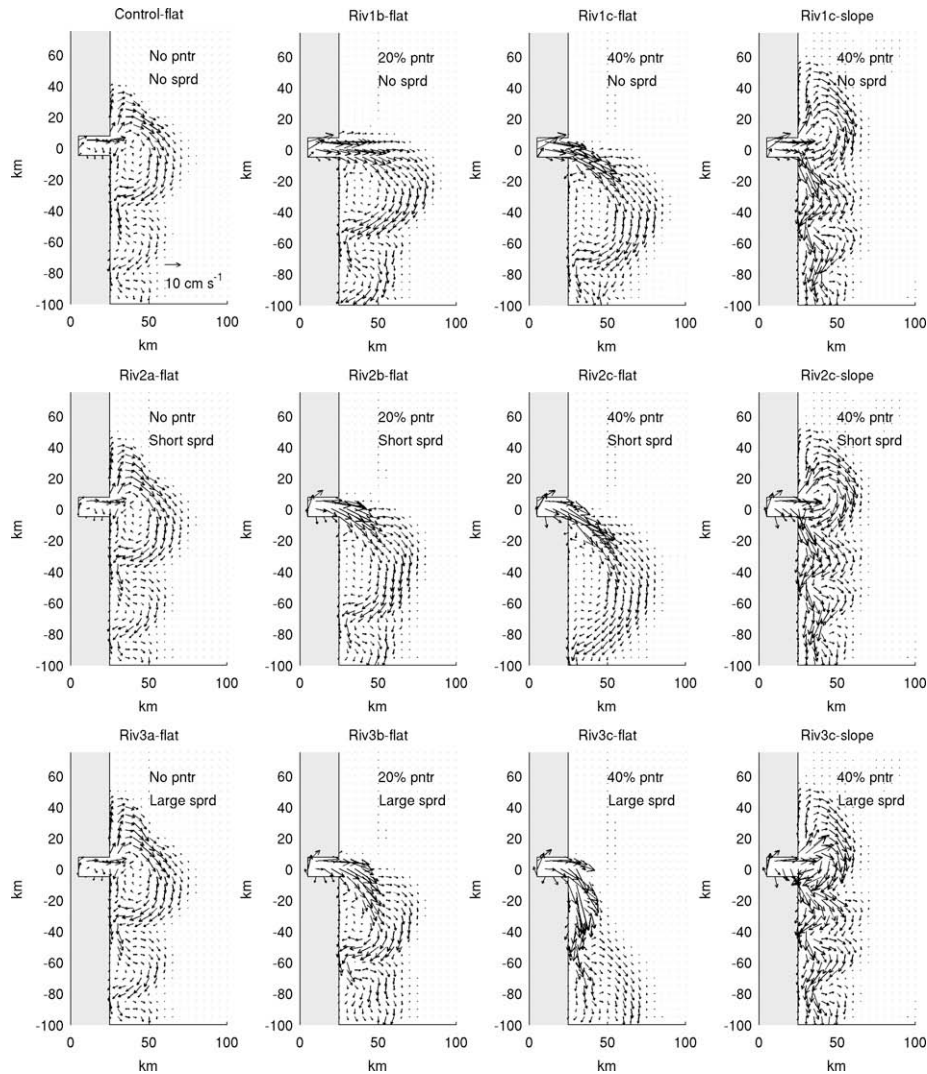


Fig. 5. Near surface velocity vectors from experiments with variable distribution of river inflow inside the estuary, at day 60 (part of the model domain shown). Downward penetration (pntr) and horizontal spreading (sprd) configurations that characterize each experiment are presented. Vectors are plotted every other grid point for better visualization.

as well as the SSS and near surface currents (not shown). This finding suggests that the vertical eddy mixing coefficients computed by each scheme are approximately the same and that vertical mixing is being controlled by the same process. In this study, two common components of the ocean interior mixing should be important: the unresolved background internal wave mixing and shear instability. In HYCOM and for all vertical mixing schemes employed here, the background internal wave mixing is parameterized through constant coefficients: scalar diffusivity is equal to $10^{-5} \text{ m}^2 \text{ s}^{-1}$, whereas background viscosity is $10^{-4} \text{ m}^2 \text{ s}^{-1}$. The parameterization of shear-driven mixing depends on the choice of vertical mixing scheme, but it is commonly related to a critical Richardson number below which the parameterization is activated. The Richardson number at model interfaces from the experiments with the three different vertical mixing schemes was calculated and compared to the Richardson number threshold from each scheme (not shown). All values of the calculated Richardson number within the buoyant plume were above the critical value below which mixing occurs, which suggests that in the study experiments the parameterization of shear-induced mixing is not triggered for any choice of scheme, and that the buoyant plume vertical mixing is controlled by the background internal wave parameterization.

5. Discussion of results

5.1. Variability of outflow properties

Enhanced vertical and horizontal mixing of the river inflow inside the estuary impacted the river mouth conditions and the structure of the buoyant outflow. Fig. 7 shows across-estuary sections (along Section 2 at the estuary mouth, see Fig. 1) of Sea Surface Height (SSH), salinity and along-estuary (u) velocity for selected experiments, at day 60. As expected, progressively increasing the downward penetration of the river inflow (Riv2-a,b,c-flat) or enlarging the estuary area with enhanced K_{iw} (Mix-a,b,c-flat) generated plume outflows that were deeper and denser. A coupled upper outflow/lower inflow structure is observed, which represents the classic gravitational circulation verified in previous numerical studies (Chao, 1988a). This gravitational circulation was enhanced as the mixing of river inflow inside the estuary increased, and the upper outflow and bottom inflow increased in magnitude. This effectively enhanced the outflow transport $T_f = \int_{A_f} u dA_f$ (A_f is the upper outflow area where u is positive, see Fig. 7 for selected expts and Table 2 for all flat bottom expts). T_f increased 146% from Riv2a to Riv2b, 55% from Riv2b

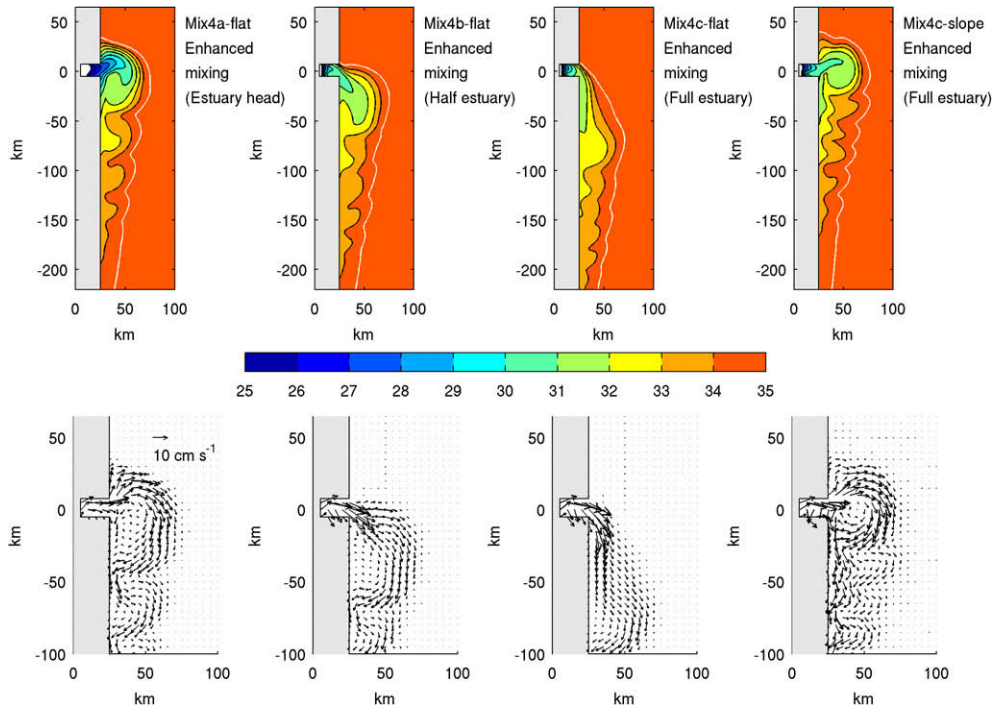


Fig. 6. Sea Surface Salinity contours (upper) and near surface velocity vectors (lower) from experiments with enhanced mixing (increased K_{iw}) inside the estuary, at day 60 (part of the model domain shown). The plume boundary (34.9) is represented by a white line. Salinity values less than 25 (inside the estuary) are not shown. The mixing information that characterizes each experiment is shown next to each plot (see Section 4.3 for details). Vectors are plotted every other grid point for better visualization.

to Riv2c, 70% from Mix4a to Mix4b and 18% from Mix4b to Mix 4c. All other “Riv” flat bottom cases present increases in T_f that are of the same order as in expts Riv2a,b,c–flat. Across-estuary (v) velocity distributions (not shown) demonstrate the development of a veering pattern of the plume outflow, which intensifies as freshwater mixing inside the estuary is enhanced. The above changes were accompanied by a progressive steepening of the salinity isolines, which was also followed by a slight steepening of the across-estuary SSH. The plume vertical structure suggests that the outflow is in geostrophic balance, which is strengthened with enhanced mixing of riverine waters inside the estuary. The presence of a bottom slope in the basin also impacted the vertical structure of the outflow. As the outflow shifted to the north side of the estuary mouth, the low-salinity area was enlarged and the isopycnals and SSH became flatter on the south side of the mouth (Riv2c–slope and Mix4c–slope). The plume outflow structure of the Control–slope case is the same as in the presence of a flat bottom. Interestingly, the slope experiments presented smaller T_f in comparison to their flat bottom counterparts (Fig. 7), which suggests a two-way interaction between the dynamics of the buoyant flow in the estuary and in the receiving basin (in Fig. 7, a comparison between Control–slope and Riv2a–flat is valid because the plume does not really change from the Riv2a–flat to the Control–flat case).

In order to summarize the main geophysical properties of the different outflows, we calculated common non-dimensional numbers from all flat bottom experiments. We concentrated on the flat bottom expts, as they facilitate comparisons to 2-layer analytical models. Such calculations involved an approximation of the plume outflow to a two-layer formulation defined by h_r , the depth where the along-estuary velocity (u) becomes negative. We defined an outflow upper layer with thickness h_1 , density ρ_1 and velocities u_1 and v_1 , and an inflow lower layer with thickness h_2 , density ρ_2 and velocities u_2 and v_2 . For each experiment, vertical profiles of u , v and ρ were extracted at the location of the core of the surface outflow at the estuary mouth; ρ_1 , ρ_2 , u_1 , u_2 , v_1 and v_2 were calcu-

lated as vertical mean values from the model grid points that are within each layer h_1 and h_2 (above and below h_r , respectively) and are presented in Table 2. These calculations did not involve averages in the across-estuary direction because in some cases the outflow velocity field is clearly concentrated on one side of the estuary channel and an average in the y direction would underestimate the outflow velocity. We calculated the gradient Richardson number $Ri = N^2/S^2$, the Froude number $Fr = |\bar{V}_1|/c_i$, the inlet Rossby number $Ro_i = |\bar{V}_1|/(fW)$ and the inlet Kelvin number $K_i = W/R_{di}$. $N^2 = (-g/\rho_0)(\rho_1 - \rho_2)/\Delta z$ is the squared stratification frequency, $S^2 = (u_1 - u_2/\Delta z)^2 + (v_1 - v_2/\Delta z)^2$ is the squared velocity vertical shear, $c_i = \sqrt{g'(h_1 \times h_2)/(h_1 + h_2)}$ is the phase speed of long internal gravity waves and $R_{di} = c_i/f$ is the internal radius of deformation; $g' = g \times (\rho_2 - \rho_1)/\rho_0$ is the reduced gravity, g is the gravitational acceleration (9.806 m s^{-2}), ρ_0 is the initial ambient density ($1022.40 \text{ kg m}^{-3}$), Δz is the distance from the surface ($z = 0$, axis positive upwards) down to the interface of the layers (equal to h_1); $|\bar{V}_1|$ is the length of the upper layer velocity vector, W is the estuary width (15 km) and f is the Coriolis parameter (10^{-4} s^{-1}).

The non-dimensional numbers presented in Table 3 summarize and corroborate with the properties of the distinct outflows. K_i was larger than 1 in all experiments, which indicates that the study experiments are all large scale discharges and that the dynamics at the estuary mouth are affected by the earth’s rotation. The fact that Ro_i is smaller than 1 in all experiments suggests that advection plays a secondary role in the dynamics governing the immediate vicinity of the estuary outflow. The outflows should be approximately in geostrophic balance, which is in agreement with the salinity vertical structures presented in Fig. 7 and will be explored further in the next section. Considerably large Ri (>20) was found in experiments that did not have enhanced vertical mixing of the river inflow (expts Control–flat, Riv2a,3a–flat), and progressively decreased to values below 3 (expts Riv2c,3c–flat and Mix4c–flat) as we enhanced vertical mixing (via downward penetration or lar-

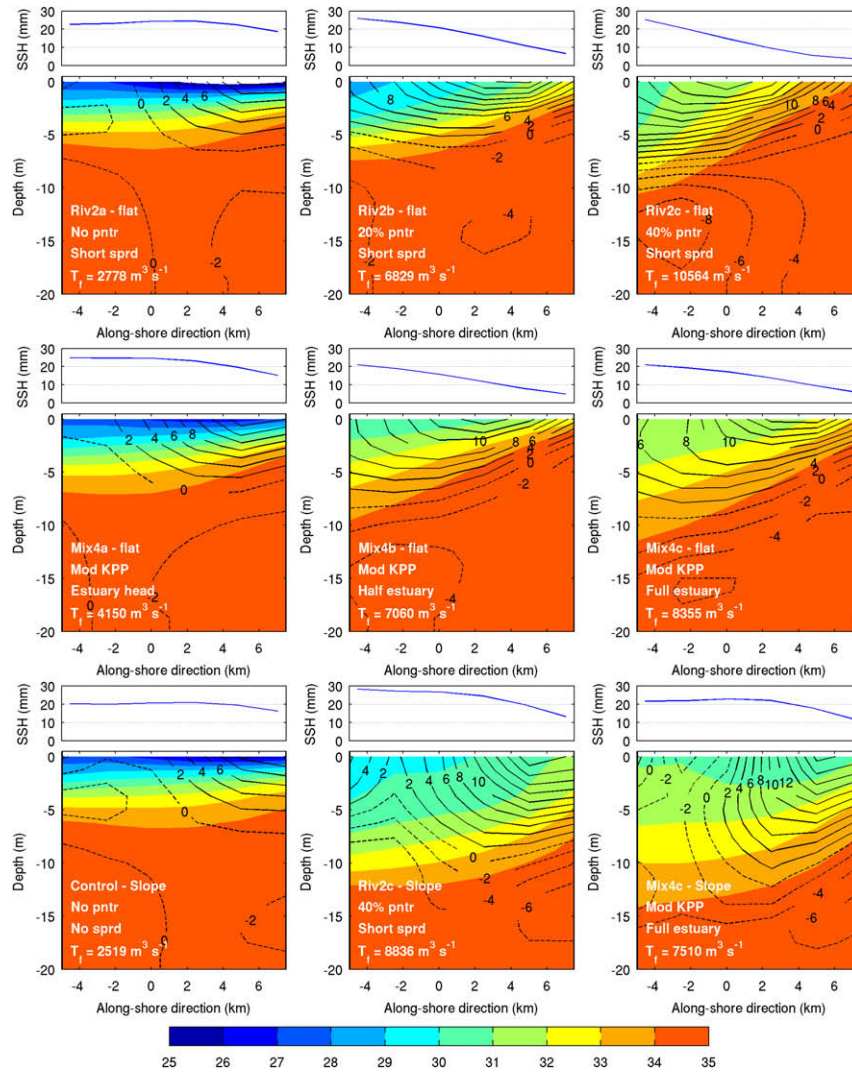


Fig. 7. Sea Surface Height (SSH, in mm), across-estuary salinity vertical structure (colors) and along-estuary velocity (u , cm s^{-1} , solid for positive/offshore and dashed for negative/onshore contours) along Section 2 (estuary mouth) from selected experiments, at day 60. The configurations that define each experiment and the outflow transport T_f for each case are shown. Salinity values less than 25 are not shown.

Table 2
Outflow transport T_f , outflow upper layer 1 and inflow lower layer 2 vertical mean values of density ρ , along-estuary (u) and across-estuary (v) velocities and layer thickness h , for all flat bottom experiments at day 60. Layers 1 and 2 average values were calculated from a vertical profile located at the core of the surface outflow at the estuary mouth. See Table 1 for attributes from experiments and Section 5.1 for details on the calculations.

Experiment	T_f ($\text{m}^3 \text{s}^{-1} \times 10^3$)	ρ_1 (sigma)	u_1 (m s^{-1})	v_1 (m s^{-1})	h_1 (m)	ρ_2 (sigma)	u_2 (m s^{-1})	v_2 (m s^{-1})	h_2 (m)
Control	2.7	19.95	0.06	0.01	6.25	22.33	-0.02	0.00	13.75
Riv1b	6.1	20.64	0.09	-0.02	6.25	22.37	-0.03	0.00	15.00
Riv1c	9.0	20.33	0.12	-0.05	7.50	22.25	-0.05	0.00	12.50
Riv2a	2.7	19.54	0.06	0.01	6.25	22.32	-0.02	0.00	13.75
Riv2b	6.8	20.54	0.12	-0.04	5.00	22.34	-0.03	0.00	15.00
Riv2c	10.5	20.59	0.13	-0.14	7.50	22.25	-0.05	0.00	12.50
Riv3a	2.7	19.41	0.06	0.01	6.25	22.32	-0.02	0.00	13.75
Riv3b	6.6	19.67	0.13	-0.03	5.00	22.30	-0.04	0.01	15.00
Riv3c	11.1	20.96	0.10	-0.05	8.75	22.31	-0.08	0.04	11.25
Mix4a	4.1	19.84	0.08	0.01	7.50	22.32	-0.03	0.00	12.50
Mix4b	7.0	20.69	0.10	-0.08	6.25	22.35	-0.03	0.00	13.75
Mix4c	8.3	21.09	0.10	-0.06	6.25	22.32	-0.05	0.02	13.75

ger K_{riv}). As expected, this was followed by an opposite behavior of Fr . Vertical stratification is important to the flow dynamics (all cases presented Fr less than one) and Fr increases with increasing downward penetration, meaning that the importance of stratifica-

tion (here measured by c_i) decreases relative to the horizontal advection of the flow. All cases fall in the category of large scale buoyant flows (Garvine, 1995) which are characterized by large K_i , small Ro_i and small Fr .

Table 3

Non-dimensional numbers calculated for all flat bottom experiments at day 60. See Table 1 for attributes from experiments. Ri : Gradient Richardson number; Fr : Froude number; Ro_i : Inlet Rossby number; K_i : Inlet Kelvin number; The internal deformation radius R_{di} (km), the squared stratification frequency N^2 ($s^{-2} \times 10^{-2}$) and the squared vertical velocity shear S^2 ($s^{-2} \times 10^{-2}$) are also shown. Numbers were calculated using values presented in Table 2. See Section 5.1 for details.

Experiment	Ri	Fr	Ro_i	K_i	R_{di}	N^2	S^2
Control	22.10	0.20	0.04	4.79	3.13	0.36	0.01
Riv1b	6.82	0.35	0.06	5.62	2.67	0.26	0.04
Riv1c	4.40	0.44	0.09	5.10	2.94	0.24	0.05
Riv2a	24.24	0.19	0.04	4.43	3.38	0.43	0.02
Riv2b	3.30	0.50	0.08	5.89	2.54	0.34	0.10
Riv2c	2.07	0.71	0.13	5.50	2.73	0.21	0.10
Riv3a	25.29	0.18	0.04	4.33	3.46	0.45	0.02
Riv3b	3.63	0.45	0.09	4.87	3.08	0.50	0.14
Riv3c	2.80	0.45	0.08	5.95	2.52	0.15	0.05
Mix4a	16.17	0.23	0.05	4.49	3.34	0.32	0.02
Mix4b	4.17	0.50	0.09	5.74	2.61	0.25	0.06
Mix4c	2.75	0.50	0.07	6.66	2.25	0.19	0.07

Certain relationships between the non-dimensional numbers, outflow properties and plume length scales are observed. As expected, stronger outflow transports (T_f) were associated with smaller Ri values (enhanced turbulent mixing and intensified estuarine gravitational circulation) which also led to stronger coastal current signals and longer downstream intrusions. Moreover, the degree of upstream intrusion was related to the buoyancy of the outflow. In the experiments that had only horizontal redistribution of the river inflow (expts Control–flat, Riv2a,3a–flat), longer upstream penetrations were observed with larger buoyancy (smaller vertical turbulent mixing, larger Ri). All other experiments that had less buoyant outflows presented no upstream intrusion. Chapman and Lentz (1994) reported the same relationship, where the rate of upstream movement of a plume was highly dependent on the outflow density anomaly. Finally, results suggest a positive relationship between the turning of the outflow and K_i . The anticyclonic turning of the outflow became stronger when K_i progressively increased, which happened with increasing vertical mixing throughout the estuary (expts Riv3a,b,c–flat and Mix4a,b,c–flat).

5.2. Dynamical balance of the outflow

As mentioned before, all experiments reproduced large-scale plume outflows because the inlet Kelvin number (K_i) was always larger than 1 (Table 3). The low inlet Rossby number (Ro_i) conditions and the vertical structure of the outflows (Fig. 7) suggest that the dynamical balance at the estuary mouth is (at a first order) geostrophic and that the outflow is in thermal wind balance. The steepening of the salinity isolines with increasing vertical mixing of freshwater (flat bottom experiments) also suggests an intensification of the geostrophic balance. Major terms of the momentum balance were computed at the location of the core of the near surface outflow (estuary mouth) and the predominant balance was geostrophic as shown by the length of each of the vectors $|c\bar{c}r| = \sqrt{(-fv)^2 + (fu)^2}$ and $|p\bar{g}f| = \sqrt{(-\rho_0^{-1}\partial p/\partial x)^2 + (-\rho_0^{-1}\partial p/\partial y)^2}$ in Fig. 8. The term $|ac\bar{c}el| = \sqrt{(Du/Dt)^2 + (Dv/Dt)^2}$ is also presented in Fig. 8, exhibiting minimal contribution to the momentum balance. In agreement with the across-estuary section from Fig. 7, the magnitude of the geostrophic balance terms increased as the vertical mixing of freshwater was enhanced (expts Riv2a,b,c–flat). In the case of expts Mix4a,b,c–flat, the difference between the pressure gradient and the Coriolis forces increased (as shown in Mix4c–flat), which

is followed by the increased contribution of the acceleration term. Although the buoyant outflow evolved into a different configuration in the presence of a bottom slope (Figs. 5 and 6), the geostrophic character of the surface outflow did not change (Riv2c–slope and Mix4c–slope).

Because this is a zonal estuary, the primary geostrophic balance of the outflow is in the across-estuary (y) direction ($fu = -\rho_0^{-1}\partial p/\partial y$). The development of the anticyclonic turning as vertical mixing of estuarine waters is increased (Figs. 5 and 6) suggests that the outflow also develops a geostrophic balance in the along-estuary (x) direction ($-fv = -\rho_0^{-1}\partial p/\partial x$). The geostrophic balance components in each direction (x and y) normalized by their respective vector lengths ($|cor_x|/|c\bar{c}r|$, $|cor_y|/|c\bar{c}r|$, $|pgf_x|/|p\bar{g}f|$ and $|pgf_y|/|p\bar{g}f|$, Fig. 8) show that the relative importance of the along-estuary components (x direction) indeed increased with enhanced mixing in all cases. This was followed by a slight decrease in the relative importance of the across-estuary components (y direction). The development of the along-estuary balance was suppressed in the presence of a sloping bottom (Riv2c–slope and Mix4c–slope), which corroborates with the lack of an anticyclonic veering by the outflow. Finally, the velocity contours and T_f values from Fig. 7 suggest that the intensification of the estuarine gravitational circulation with enhanced freshwater mixing must be accompanied by an increase in the upward entrainment from the bottom inflow to the surface outflow. Average upward velocities inside the estuary (Fig. 8) confirmed this pattern and show that they can be six times larger in the presence of enhanced freshwater mixing (expts Riv2a,c–flat). Very interestingly, the bottom slope worked against this intensification and promoted vertical velocities that were slightly smaller (Riv2c–flat and Riv2c–slope), as well as smaller T_f values (Fig. 7). The average negative vertical velocity became more negative with increased vertical mixing, meaning that downward motions were also enhanced. The concomitant increase of both upward and downward motions suggests that the estuarine secondary circulation was intensified.

5.3. Topographic constrains on the development and transport of plume waters

The most pronounced impact of the bottom slope over the structure of the buoyant plume was the restriction of the offshore development and changes in the shape and position of the recirculating bulge (Figs. 5 and 6). The bottom slope greatly impacted the buoyant outflow conditions at the river mouth, even though the estuary was still at flat bottom and only the “shelf” had varying topography. In particular, the outflow did not develop an anticyclonic veering when it encompassed the sloping bottom (expts Riv1c,2c,3c–slope and Mix4c–slope).

The question suggested by these findings is: How does the bottom slope change the properties of the geostrophic buoyant outflow and how does that affect the development of the anticyclonic bulge? This question is tackled by investigating the evolution of the buoyant plume in expts Riv2c–flat and Riv2c–slope. A series of snapshots of near surface velocity vectors (Fig. 9) reveals that the surface plume “feels” the sloping bottom in its early stage of development. The buoyant outflow gradually shifted from a configuration with an anticyclonic veering to a configuration where it exited the estuary in a straight path and was concentrated on the northern side of the mouth. This pattern was accompanied by the development of a bulge in front of the estuary. This development was very different in the presence of a flat bottom, where the outflow maintained an anticyclonic veering configuration and exited the estuary as jet that was free to expand offshore, which ultimately led to the development of a large bulge south of the river mouth. These changes in the buoyant outflow circulation also reflected modifications in the surface relative

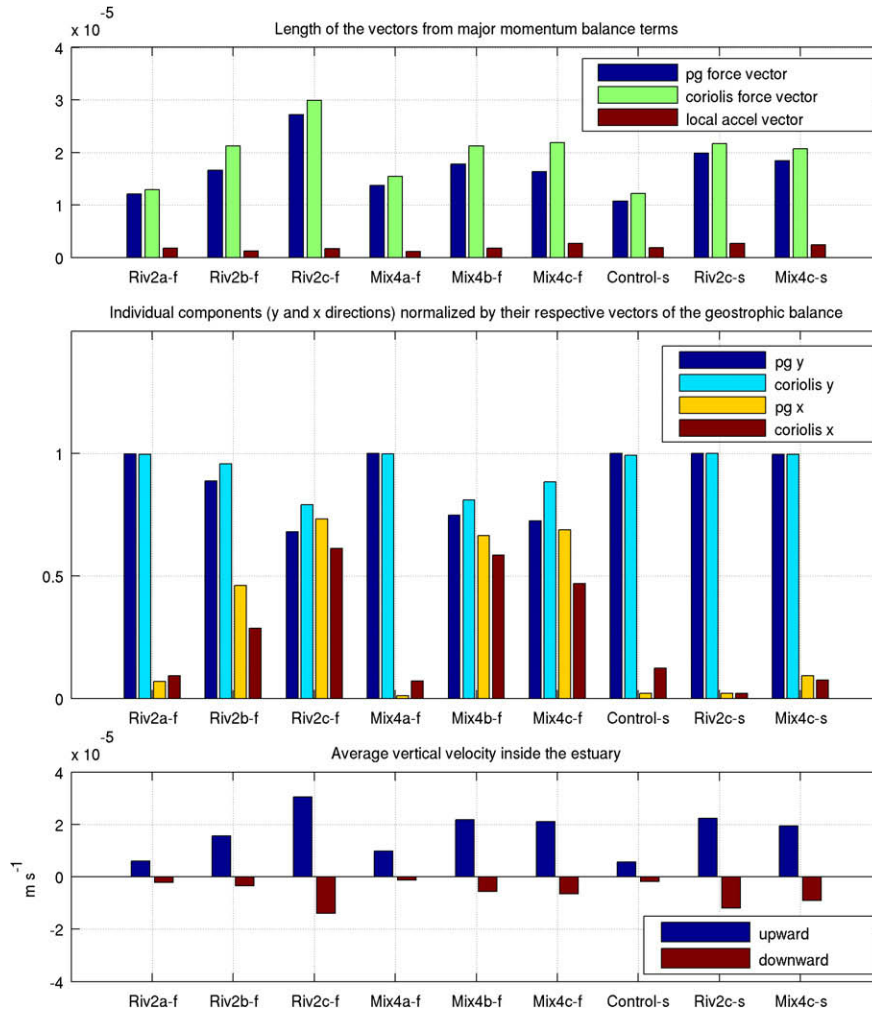


Fig. 8. (Upper) Magnitude of each of the major momentum balance vectors ($|c\bar{or}| = \sqrt{(-fv)^2 + (fu)^2}$, $|p\bar{g}f| = \sqrt{(-\rho_0^{-1}\partial p/\partial x)^2 + (-\rho_0^{-1}\partial p/\partial y)^2}$ and $|ac\bar{cel}| = \sqrt{(Du/Dt)^2 + (Dv/Dt)^2}$ where $D(u, v)/Dt = \partial(u, v)/\partial t + \vec{V} \cdot \nabla(u, v)$) from selected experiments. Values were extracted from Section 2 (estuary mouth) at the location of the near surface outflow core, at day 60. (Middle) Correspondent individual components of each geostrophic balance term normalized by the associated vector length ($|cor_x|/|c\bar{or}|$, $|cor_y|/|c\bar{or}|$, $|pgf_x|/|p\bar{g}f|$ and $|pgf_y|/|p\bar{g}f|$). (Lower) Average positive (upward) and negative (downward) vertical velocity inside the estuary, at day 60.

vorticity $\zeta = (\partial v/\partial x) - (\partial u/\partial y)$ (Fig. 10) in the vicinity of the river mouth (along Section 3 in the vicinity of the estuary, Fig. 1). In the presence of a flat bottom, the ζ field remained constant throughout time and reflected the buoyant outflow jet with opposite ζ signals on each side of the flow. When the bottom slope was employed, ζ progressively changed in time and reflected the development of the recirculating bulge with a negative signal (anticyclonic) that is surrounded by positive signals to the north (cyclonic turning of the upstream intrusion) and to the south (cyclonic turning of the bulge intrusion at the coast), followed by a negative signal associated with a coastal current meander (see Fig. 5).

Numerical experiments performed by Chao (1988a) and Kourafalou et al. (1996) investigated the impact of a sloping bottom on the structure of the river plume in a domain configuration similar to the one in this study (rectangular basin, idealized flat bottom estuary and gentle slope starting at the coast). Their results demonstrate that the bottom slope induced gain in anticyclonic vorticity for the plume due to enhanced upwelling and surface divergence. The higher surface elevation near the river mouth increased the along-shore (sloping northward) pressure gradient which enhanced the north extension of the plume, while the increased shoreward flow south of the mouth produced a stronger southward coastal current. Fig. 9 suggests that this upstream shift is triggered as soon as the buoyant plume reaches the basin, be-

tween 5 and 10 days. Hovmöller diagrams of vertical velocity in the vicinity of the estuary mouth (also along Section 3) demonstrate the differences in the vertical velocity pattern between flat and slope conditions (Fig. 10). Until approximately 10 days, the vertical velocity field from the flat and slope conditions were similar, although enhanced upwelling was observed in the presence of the slope. Both fields start to diverge after 10 days which is a result from the development of different circulation patterns. In flat bottom conditions, the vertical velocity field was characterized by a downwelling fringe around the bulge and an upwelling signal inside it (the section only captures the northern part of the bulge). In the presence of a slope, the upwelling signal inside the bulge (red region) was considerably stronger, which was followed by a strong downwelling signal (blue region) where the bulge circulation turns cyclonically to feed the coastal current, the latter presenting an upwelling signal (yellow region) associated with the meandering of the coastal current. This comparison suggests that indeed the enhanced upwelling is related to the northward displacement of the bulge, which could shift the buoyant outflow to a different configuration. This pattern is also observed in the expts Riv1c,3c-slope and Mix4c-slope and to a less degree in the Control-slope case (not shown).

The position of the offshore edge of the plume in time is compared between selected slope experiments and their flat bottom

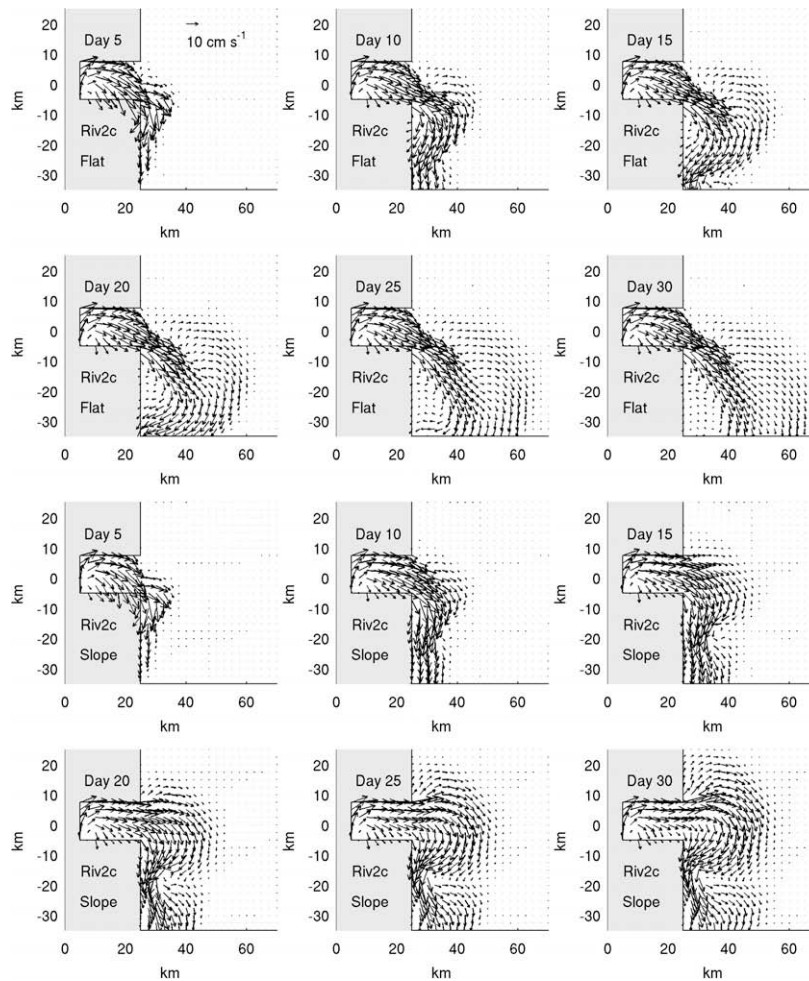


Fig. 9. Snapshots of near surface velocity vectors from Riv2c experiments (from both flat and sloping bottom conditions) starting on day 5 to day 30, every 5 days (part of the model domain shown). Vectors are plotted every other grid point for better visualization.

counterparts (Fig. 11). Apart from the Control cases, the recirculating bulges in flat and sloping bottom conditions started to diverge from each other around day 15 and the bottom slope imposed significant upstream displacements of the bulge after 60 days. The above changes in the recirculating bulge also impacted coastal current properties such as the displacement of the coastal current nose and the integrated transport ($\text{m}^3 \text{s}^{-1}$), which is defined as the downstream, along-shore (v) transport at $y = -127.5 \text{ km}$ integrated in time (Fig. 12). The bottom slope promoted a longer coastal current region, and the most pronounced differences were observed between Riv2c–Slope and Riv2c–flat, the former presenting a coastal current that is 50 km longer and an integrated transport that is $75,000 \text{ m}^3 \text{ s}^{-1}$ larger than the latter (after 60 days). On the other hand, the experiment Mix4c–slope presented a coastal current that is slightly shorter and with a smaller transport than the one in Mix4c–flat, a fact that could be attributed to the large upstream displacement of the plume by the bottom slope.

5.4. Plume development in hybrid coordinate layers

In applying the HYCOM model on the idealized basin that includes “coastal” and “offshore” settings, it is important to consider if the choice of vertical coordinates can impact the plume dynamics, namely the along-shore and across-shore evolution of the plume and its vertical structure. Therefore, we explored the hybrid layer capability of the model and reproduced all slope experiments

with two additional vertical coordinate configurations. In the first case, we substituted the standard cartesian–isopycnal configuration with purely sigma coordinates. Thirty sigma levels were imposed with thicknesses ranging from 0.66 m in the estuary and near the coastline to 3.33 m in deep water. In the second case, a sigma–isopycnal configuration was imposed. Twenty-four sigma levels were prescribed in the first 48 m of depth (thicknesses ranging from 0.83 m in the estuary and near the coastline to 2 m in deep water) which laid on top of 6 deep isopycnal levels. In both configurations, the sigma levels were set to remain fixed, i.e. they could not transform to isopycnal layers.

Salinity horizontal (near surface) distributions and vertical across-shore sections for a selected experiment (Riv2c–slope) employing its standard vertical coordinate configuration (cartesian–isopycnal) and using the two new cases (sigma-only and sigma–isopycnal) are presented in Fig. 13. In all cases we found that the plume vertical and horizontal structures are not impacted by the hybrid vertical coordinate choices. In the cases with 2 types of layers (cartesian–isopycnal and sigma–isopycnal), the upper ocean region where the fixed levels were imposed was always deeper than the plume region (buoyant plume and bottom undercurrent), which was a necessary measure to ensure proper vertical resolution of the plume structure. The choice of the depth that defines the region of permanent fixed levels was critical. Results from experiments where isopycnal layers could reach 10 m below the surface or less (not shown) had isopycnals interacting with the

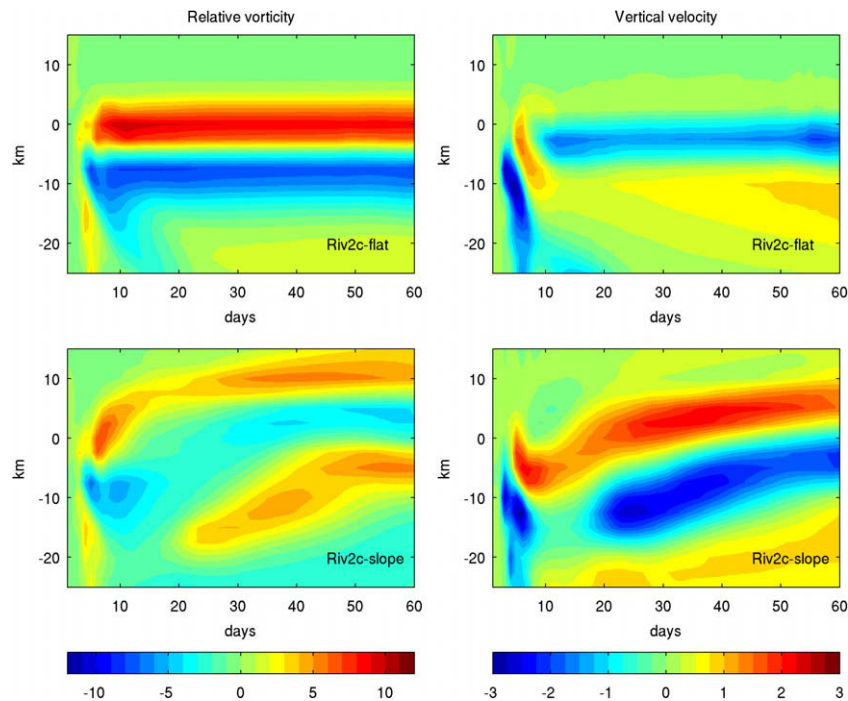


Fig. 10. Hovmöller diagrams of surface relative vorticity $\zeta = (\partial v/\partial x) - (\partial u/\partial y)$ ($s^{-1} \times 10^{-5}$, left panels) and of vertical velocity ($m s^{-1} \times 10^{-5}$) at 15 m below the surface (model layer 12, right panels) from the Riv2c experiments (upper: flat bottom, lower: sloping bottom) along Section 3 (vicinity of the estuary).

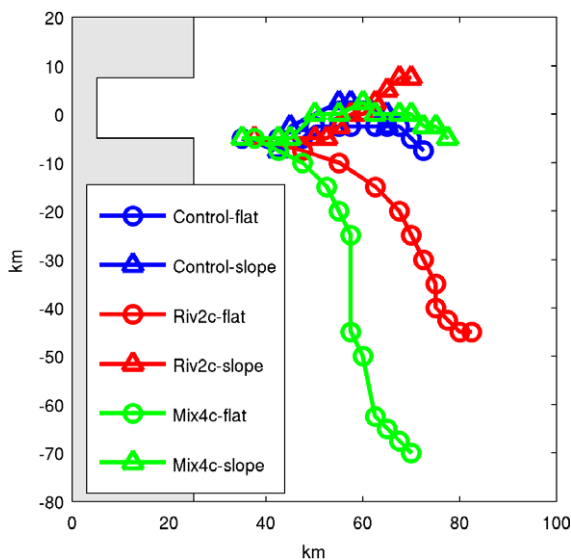


Fig. 11. Locations of the offshore edge of the recirculating bulge from selected pairs of flat and sloping bottom experiments (Control, Riv2c and Mix4c). Positions are shown every 5 days for better visualization.

bottom of the buoyant plume, which was detrimental for the vertical structure of the plume. The flexibility that vertical coordinates have to transform to fixed (cartesian/sigma) or isopycnal layers is a powerful tool to provide the best vertical resolution for different ocean processes. However, for the purposes of this study (which involves a freshwater source, hence a process that continually changes density at the surface), it was equally important to maintain the surface layers as fixed levels at all times (i.e., permanent cartesian/sigma levels that cannot transform to isopycnal layers) in order to ensure adequate resolution.

Hybrid coordinate issues have been previously addressed by Winther and Evensen (2006), who tested three different vertical level configurations (involving cartesian and sigma coordinates) on numerical simulations of the shelf/shelf-break circulation and water masses formation in the North Sea and Skagerrak region. They concluded that model results from each configuration did not differ considerably from each other; they employed comparison with in situ and satellite data to evaluate model errors associated with the model set-up and properties of the vertical mixing scheme. When employing a hybrid structure and a nested approach with HYCOM to study coastal processes beyond the purely buoyancy-driven problem addressed in this study, vertical resolution is an important issue (Halliwell et al., 2009). Large scale models in HYCOM (global and basin-wide) used to extract boundary conditions employ a vertical coordinate strategy in the stratified open ocean that limits the thickness of the near-surface fixed coordinate domain and maximizes the ocean region represented by isopycnal coordinates. This strategy usually provides poor vertical resolution over the middle/outer continental shelf so that the bottom boundary layer cannot be resolved in the outer, larger scale domain and is detrimental for nested coastal models. It is, therefore, advisable to expand the near-surface fixed coordinate domain in the outer model fields by adding additional layers before nesting to the coastal domain.

6. Summary and concluding remarks

Previous numerical modeling and laboratory experiments have shown that the development of the recirculating bulge and properties of the coastal current are sensitive to different conditions at the source of freshwater, such as the momentum, buoyancy and overall outflow transport (Yankovsky and Chapman, 1997; Garvine, 1999; Fong and Geyer, 2002), the angle of the buoyant outflow with the coast line (Garvine, 2001; Avicola and Huq, 2003a,b) and the actual river boundary conditions in numerical

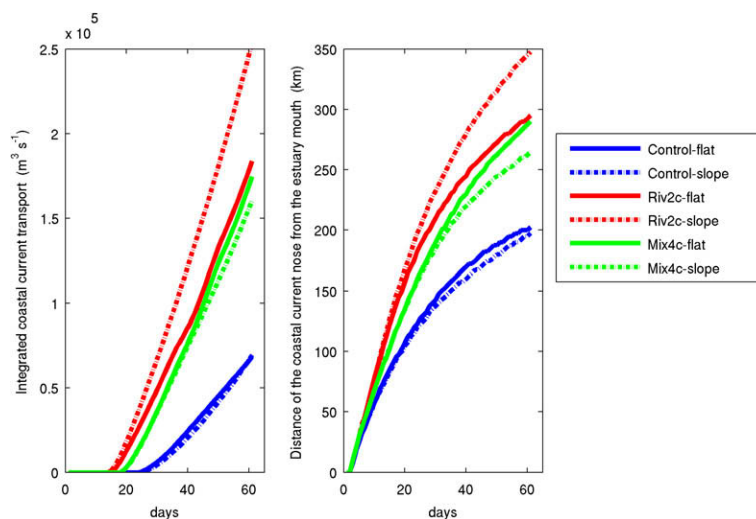


Fig. 12. Time series of integrated downstream coastal current transport ($\text{m}^3 \text{s}^{-1}$, left) and displacement of the coastal current nose (km, right) away from the estuary mouth from selected pairs of flat and sloping bottom experiments (Control, Riv2c and Mix4c). Coastal current transports were calculated at an across-shore section 127.5 km south of the estuary.

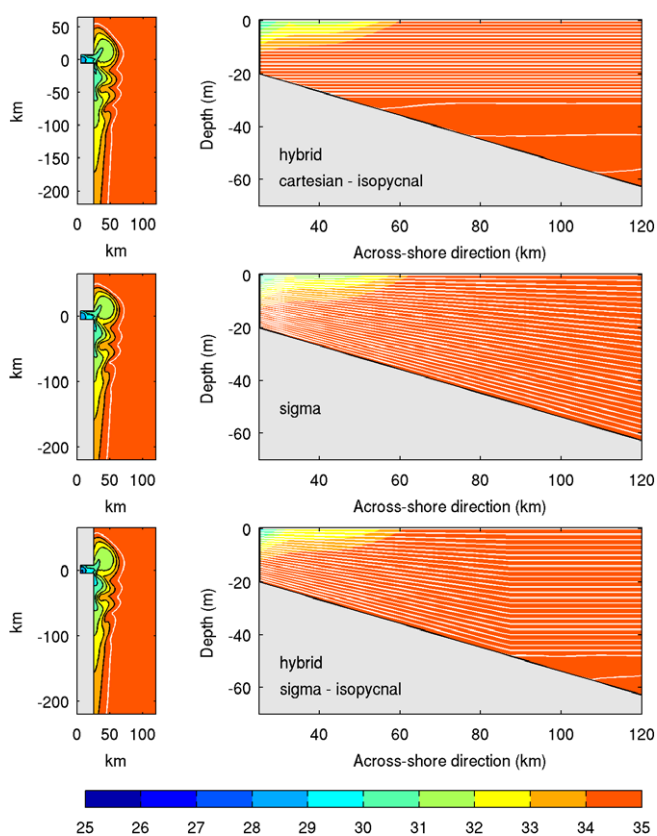


Fig. 13. (Right) Cross-shore salinity vertical structure along Section 1 (across the basin), starting at the estuary mouth (where the slope starts) from the Riv2c-slope experiment with three different vertical layers setting, at day 60. (Upper) cartesian-isopycnal. (Middle) sigma only. (Lower) sigma-isopycnal. Layer interfaces are shown as solid white lines. Left: Corresponding Sea Surface Salinity field, for each case. The plume boundary (34.9) is represented by a white line.

models (Yankovsky, 2000; Garvine, 2001). The study presented herein was designed to investigate how the variability in the structure of a river plume is connected to changes in the vertical mixing of riverine waters inside an estuary-like source. Although we did not elaborate on details of estuarine dynamics and in spite of the

simplified model configuration, it was demonstrated that the dynamics of the flow prior to reaching the receiving basin play an important role on the properties of the buoyant plume in a flat bottom basin. Our results show that increased vertical and horizontal mixing of freshwater inside the estuary enhanced the estuarine gravitational circulation and led to stronger and less buoyant outflows that developed a consistent anticyclonic veering at the river mouth. This shift in the outflow properties clearly impacted the near (bulge) and far (coastal current) fields of the plume, since it led to the development of river plumes that varied between having smaller bulges with a coherent upstream intrusion, or presenting large and circular bulges with no upstream intrusion or not even developing a coherent bulge, as all outflow was deflected in the downstream direction.

The impact of the earth's rotation on estuarine/bay dynamics has been modeled in different large scale systems (Valle-Levinson et al., 1996, 2007; Kourafalou, 2001; Soares et al., 2007a,b). Chao and Boicourt (1986) and Chao (1988a) demonstrated that under the effect of the earth's rotation, the upward entrainment caused by the estuarine gravitational circulation will induce an anticyclonic shear on the surface estuarine circulation, a cyclonic shear on the bottom inflow and the development of an S-shaped secondary circulation. Moreover, the plume outflow should be in approximate geostrophic balance (for low Ekman and Rossby numbers) with the development of a Margules density front at the estuary mouth. This pattern is observed in our simulations and resembles the vertical structure of a large scale estuary such as the Delaware Bay (Münchow and Garvine, 1993b; Sanders and Garvine, 2001). Our results expand on previous findings by showing that the strength and direction of this geostrophic outflow are dependent on the degree of freshwater vertical mixing inside the estuary. As this mixing was enlarged, there was an increase in the average upward vertical velocity inside the estuary. This shift, in accordance to Chao (1988a), was concomitant with an intensification of the geostrophic outflow and an enhancement of the anticyclonic veering at the estuary mouth. Changes in the outflow angle (the angle the outflow makes with the coastline) have been related to the geometry and orientation of the estuary/bay previously (Garvine, 2001; Avicola and Huq, 2003a,b). The present study demonstrated that this angle is also dependent on the estuarine dynamics.

The development of the river plume in the presence of a sloping bottom is in agreement with previous studies (Chao, 1988a; Koura-

alou et al., 1996; Garvine, 1999) as well as with observations on topographic effects on plume development (Valle-Levinson et al., 2007). Our results highlight that the impact of changing the estuarine mixing conditions was greatly minimized when the buoyant plumes developed in the presence of a gentle sloping bottom. Although the plumes were not in contact with the bottom (surface-advected plumes), their development was affected by the bottom slope. This was especially evident in the case of plumes that were very distinct in the flat bottom domain experiments, but developed very similar features in the presence of a sloping bottom. The largest impacts were in the shift of the recirculating bulge in the upstream direction and in the subsequent change in the configuration of the outflow. Very interestingly, these impacts appear to transmit changes into the estuary, since the buoyant outflow T_f decreased together with a slight decay in the average estuarine vertical velocity in comparison to the same experiments in the flat bottom basin (Figs. 7 and 8).

Although our approach is idealized (box-like domain with simple estuary, flat or gently sloping bottom and no external forcing), the results presented here demonstrate that a two-way interaction may exist between the buoyant plume and the estuarine circulation and that both should be considered as part of a single system (MacCready et al., 2009). It is important to emphasize that this study is in the context of large-scale estuaries ($K_i > 1$) where the effects of rotation are part of the estuarine dynamics. These concepts may not be applicable to narrow estuaries ($K_i < 1$), where constrictions (lateral jetties, sills) that act as hydraulic controls in the estuarine channel may have a profound impact on the plume outflow (Hetland, 2005; MacDonald and Geyer, 2004; MacDonald et al., 2007; MacCabe et al., 2008). Our assumption of no temperature difference between river inflow and shelf is generally valid, as river plume dynamics are controlled by the salinity gradients. However, strong coastal temperature gradients imposed either by a cold discharge or by increased cooling of the shallow portion of the shelf due to cold air outbreaks can have implications for density-driven coastal currents. An example is the West Adriatic Coastal Current which is largely driven by river runoff, with the exception of the winter season, when it becomes barotropic (wind-driven), due to compensation of the temperature and salinity gradients in the density field (Zavatarelli et al., 2002).

The choice of vertical coordinate (fully cartesian, fully sigma, cartesian–isopycnal, sigma–isopycnal) did not induce major changes in the vertical structure of the plume, although having a number of near surface layers that are permanently cartesian/sigma levels was necessary to ensure the vertical resolution of the plume. Isopycnal layers cannot change their assigned density, and therefore they can be detrimental to the vertical resolution of the buoyant plume in case it interacts with them. Based on our results, it is recommended that isopycnal layers should remain well below the bottom of the buoyant plume. More generally, the choice for this “minimum isopycnal depth” should be carefully determined by the user and is undoubtedly dependent on the process under study, the forcing mechanisms and the general framework of the simulations (process-oriented or realistic). The choice of hybrid layers is a beneficial model feature for realistic simulations with variable bathymetry, where the inner-shelf is connected to deeper shelf areas and to the open ocean. Numerical experiments within such a realistic framework should provide a full assessment of the impacts of hybrid layers over the dynamics of coastal buoyant plumes, and their interactions with shelf-break/deep ocean features.

In conclusion, the study revealed the influence of estuarine horizontal and vertical stratification on the outflow properties and on the overall plume structure, as it evolves on the continental shelf. The understanding of the related processes is expected to provide a contribution to realistic studies. The HYCOM model was capable to

reproduce major processes in river plume dynamics that control the flow field associated with the spreading of buoyant waters, in the absence of external forcing. Future studies involving processes associated with ambient currents, winds and tides are necessary to address the full model capabilities to simulate more complex coastal dynamics associated with buoyant flows of river origin on continental shelves.

Acknowledgments

This study was funded by the Office of Naval Research (N000140510892; N000140810980) and the National Science Foundation (OCE-0929651). We are grateful to Alan Wallcraft (NRL-SSC) for coding support to develop the river plume parameterization options presented herein and implement them in the latest HYCOM code release. We thank three anonymous reviewers for their careful evaluation of the manuscript and their constructive comments.

References

- Avicola, G., Huq, P., 2003a. The role of outflow geometry in the formation of the recirculating bulge region in coastal buoyant outflows. *Journal of Marine Research* 61, 411–434.
- Avicola, G., Huq, P., 2003b. The characteristics of the recirculating bulge region in coastal buoyant outflows. *Journal of Marine Research* 61, 435–463.
- Blanton, J.O., Werner, F., Kim, C., Atkinson, L., Lee, T., Savidge, D., 1994. Transport and fate of low-density water in a coastal zone. *Continental Shelf Research* 14, 401–427.
- Bleck, R., Boudra, D., 1981. Initial testing of numerical ocean circulation model using a hybrid (quasi-isopycnic) vertical coordinate. *Journal of Physical Oceanography* 11, 755–770.
- Bleck, R., Smith, L.T., 1990. A wind-driven isopycnic coordinate model of the north and equatorial atlantic ocean 1. Model development and supporting experiments. *Journal of Geophysical Research* 95 (C3), 3273–3285.
- Bleck, R., Rooth, C., Hu, D., Smith, L., 1992. Salinity-driven thermocline transients in a wind- and thermohaline-forced isopycnic coordinate model of the North Atlantic. *Journal of Physical Oceanography* 22, 1486–1505.
- Bleck, R., Benjamin, S., 1993. Regional weather prediction with a model combining terrain-following and isentropic coordinates. *Monthly Weather Review* 121, 1770–1785.
- Bleck, R., 2002. An oceanic circulation model framed in hybrid isopycnic–Cartesian coordinates. *Ocean Modelling* 37, 55–88.
- Boicourt, W.C., 1973. The Circulation of Water on the Continental Shelf from Chesapeake Bay to Cape Hatteras. PhD thesis. The Johns Hopkins University.
- Browning, G.L., Kreiss, H.-O., 1982. Initialization of the shallow water equations with open boundaries by the bounded derivative method. *Tellus* 34, 334–351.
- Browning, G.L., Kreiss, H.-O., 1986. Scaling and computation of smooth atmospheric boundary conditions. *Tellus* 38A, 295–313.
- Canuto, V.M., Howard, A., Cheng, Y., Dubovikov, M.S., 2001. Ocean turbulence part I: one-point closure model, momentum and heat vertical diffusivities. *Journal of Physical Oceanography* 31, 1413–1426.
- Canuto, V.M., Howard, A., Cheng, Y., Dubovikov, M.S., 2002. Ocean turbulence part II: vertical diffusivities of momentum, heat, salt, mass and passive scalars. *Journal of Physical Oceanography* 32, 240–264.
- Chant, R.J., Glenn, S.M., Hunter, E., Kohut, J., Chen, R.F., Houghton, R.W., Bosh, J., Schofield, O., 2008. Bulge formation on a buoyant river flow. *Journal of Geophysical Research* 113, C01017. doi:10.1029/2007JC004100.
- Chao, S.Y., Boicourt, W.C., 1986. Onset of estuarine plumes. *Journal of Physical Oceanography* 16, 2137–2149.
- Chao, S.Y., 1988a. River-forced estuarine plumes. *Journal of Physical Oceanography* 18, 72–88.
- Chao, S.Y., 1988b. Wind-driven motion of estuarine plumes. *Journal of Physical Oceanography* 18, 1144–1166.
- Chapman, D.C., Lentz, S.J., 1994. Trapping of a coastal density front by the bottom boundary layer. *Journal of Physical Oceanography* 24, 1464–1479.
- Chassignet, E.P., Smith, L.T., Halliwell, G.R., 2003. North atlantic simulations with the hybrid coordinate ocean model (HYCOM): impact of the vertical coordinate choice, reference pressure and thermobaricity. *Journal of Physical Oceanography* 33, 2504–2526.
- Chassignet, E.P., Hurlburt, H.E., Smedstad, O.M., Halliwell, G.H., Wallcraft, A.J., Metzger, E.J., Blanton, B.O., Lozano, C., Rao, D.B., Hogan, P.J., Srinivasan, A., 2006. Generalized vertical coordinates for eddy-resolving global and coastal ocean forecasts. *Oceanography* 19 (1), 20–31.
- Fong, D.A., Geyer, W.R., 2002. The alongshore transport of freshwater in a surface-trapped river plume. *Journal of Physical Oceanography* 32, 957–972.
- Garvine, R.W., 1987. Estuary plumes and fronts in shelf waters: a layer model. *Journal of Physical Oceanography* 17, 1877–1896.
- Garvine, R.W., 1995. A dynamical system for classifying buoyant coastal discharges. *Continental Shelf Research* 15 (13), 1585–1596.

- Garvine, R.W., 1999. Penetration of buoyant coastal discharge onto the continental shelf: a numerical model experiment. *Journal of Physical Oceanography* 29, 1892–1909.
- Garvine, R.W., 2001. The impact of model configuration in studies of buoyant coastal discharge. *Journal of Marine Research* 59, 193–225.
- Griffiths, R.W., Hopfinger, E.J., 1983. Gravity currents along a lateral boundary in a rotating fluid. *Journal of Fluid Mechanics* 134, 357–399.
- Halliwel, G.R., 2004. Evaluation of vertical coordinate and vertical mixing algorithms in the HYbrid-Coordinate Ocean Model (HYCOM). *Ocean Modelling* 7, 285–322.
- Halliwel, G.R., Weisberg, R.H., Mayers, D.A., 2003. A synthetic float analysis of upper-limb meridional overturning circulation interior ocean pathways in the tropical/subtropical Atlantic. In: Malanotte-Rizzoli, P., Goni, G., (Eds.). *Interhemispheric Water Exchange in the Atlantic Ocean*, Elsevier, pp. 93–136.
- Halliwel, G.R., Barth, A., Weisberg, R.H., Hogan, P., Smedstad, O.M., Cummings, J., 2009. Impact of GODAE products on nested HYCOM simulations of the West Florida Shelf. *Ocean Dynamics* 59, 139–155.
- Hetland, R.D., 2005. Relating river plume structure to vertical mixing. *Journal of Physical Oceanography* 35, 1667–1688.
- Hickey, B.M., Pietrafesa, L.J., Jay, D.A., Boicourt, W.C., 1998. The Columbia river plume study: subtidal variability in the velocity and salinity fields. *Journal of Geophysical Research* 103 (C5), 10339–10368.
- Hickey, B., Geier, S., Kachel, N., MacFadyen, A., 2005. A bi-directional river plume: the Columbia in summer. *Continental Shelf Research* 25, 1631–1656.
- Hogan, P.J., Hurlburt, H.E., 2006. Why do intra thermocline eddies form in the Japan/East Sea? A modeling perspective. *Oceanography* 19 (3), 134–143.
- Horner-Devine, A.R., Fong, D.A., Monismith, S.G., Maxworthy, T., 2006. Laboratory experiments simulating a coastal river inflow. *Journal of Fluid Mechanics* 555, 203–232.
- Horner-Devine, A.R., Fong, D.A., Monismith, S.G., 2008. Evidence for the inherent unsteadiness of a river plume: Satellite observations of the Niagara River plume. *Limnology and Oceanography* 53 (6), 2731–2737.
- Horner-Devine, A.R., 2009. The bulge circulation in the Columbia River plume. *Continental Shelf Research* 29, 234–251.
- Huang, R.W., 1993. Real freshwater flux as a natural boundary condition for the salinity balance and thermohaline circulation forced by evaporation and precipitation. *Journal of Physical Oceanography* 23, 2428–2446.
- Ikeda, M., 1984. Coastal flows driven by a local density flux. *Journal of Geophysical Research* 89 (C5), 8008–8016.
- Kao, T.W., Park, C., Pao, H.-P., 1977. Buoyant surface discharge and small-scale oceanic fronts: a numerical study. *Journal of Geophysical Research* 82 (12), 1747–1752.
- Kao, T.W., 1981. The dynamics of small scale fronts I, shelf water structure due to freshwater discharge. *Journal of Physical Oceanography* 11, 1215–1223.
- Kara, A.B., Rochford, P.A., Hurlburt, H.E., 2000. Efficient and accurate bulk parameterization of air-fluxes for use in general circulation models. *Journal of Atmospheric and Oceanic Technology* 17, 1421–1438.
- Kara, A.B., Hurlburt, H.E., Wallcraft, A.J., Bourassa, M.A., 2005. Black Sea mixed layer sensitivity to various wind and thermal forcing products on climatological time scales. *Journal of Climate* 18 (24), 5266–5293.
- Kourafalou, V.H., Oey, L.-Y., Wang, J., Lee, T., 1996. The fate of river discharge on the continental shelf Part I: modeling the river plume and the inner shelf coastal current. *Journal of Geophysical Research* 101 (C2), 3415–3434.
- Kourafalou, V.H., 2001. Modelling river plumes on Mediterranean shelves: Po River plume (North Adriatic Sea) and Axios River plume (North Aegean Sea). *Journal of Marine Systems* 30 (3–4), 181–205.
- Kourafalou, V. H., Balotro, R.S., Peng, G., Lee, T.N., Johns, E., Ortner, P., Wallcraft, A., Townsend, T., 2006. Seasonal variability of circulation and salinity around Florida Bay and the Florida Keys: SoFLA-HYCOM results and comparison with in-situ data. Technical report 2006/04, University of Miami, Miami, Florida.
- Kourafalou, V.H., Peng, G., Kang, H., Hogan, P.J., Smedstad, O.M., Weisberg, R.H., Baringer, M.O., Meinen, C.S., 2009. Evaluation of global ocean data assimilation experiment products on south florida nested simulations with the hybrid coordinate ocean model. *Ocean Dynamics* 59, 47–66.
- Large, W.G., McWilliams, J.C., Doney, S.C., 1994. Oceanic vertical mixing: a review and a model with a nonlocal boundary layer parameterization. *Reviews in Geophysics* 32, 363–403.
- MacCabe, R.M., Hickey, B.M., MacCready, P., 2008. Observational estimates of entrainment and vertical salt flux in the interior of a spreading plume. *Journal of Geophysical Research* 113, C08027. doi:10.1029/JC004361.
- MacCready, P., Banas, N.S., Hycyck, B.M., Denver, E.P., Liu, Y., 2009. A model study of tide- and wind-induced mixing in the Columbia River Estuary and plume. *Continental Shelf Research* 29, 278–291.
- MacDonald, D.G., Geyer, W.R., 2004. Turbulent energy production and entrainment at a highly stratified estuarine front. *Journal of Geophysical Research* 109, C05004. doi:10.1029/2003JC002094.
- MacDonald, D.G., Goodman, L., Hetland, R.H., 2007. Turbulent dissipation in a near-field river plume: a comparison of control volume and microstructure observations with a numerical model. *Journal of Geophysical Research* 112, C07026. doi:10.1029/JC004075.
- Marmorino, G.O., Trump, C.L., 2000. Gravity current structure of the Chesapeake Bay outflow plume. *Journal of Geophysical Research* 105 (C12), 28847–28861.
- Masse, A.K., Murthy, C.R., 1992. Analysis of the Niagara River Plume dynamics. *Journal of Geophysical Research* 97 (C2), 2403–2420.
- Mellor, G.L., Yamada, T., 1982. Development of a turbulence closure model for geophysical fluid problems. *Reviews of Geophysics and Space Physics* 20, 851–875.
- Morel, Y., Baraille, R., Pichon, A., 2008. Time splitting and linear stability of the slow part of the barotropic component. *Ocean Modelling* 23, 73–81.
- Münchow, A., Garvine, R.W., 1993a. Buoyancy and wind forcing of a coastal current. *Journal of Marine Research* 51, 293–322.
- Münchow, A., Garvine, R.W., 1993b. Dynamical properties of a buoyancy-driven coastal current. *Journal of Geophysical Research* 98 (C11), 20063–20077.
- Oey, L., Mellor, G.L., 1993. Subtidal variability of estuarine outflow plume and coastal current: a model study. *Journal of Physical Oceanography* 23, 164–171.
- Olascoaga, M.J., Rypina, I.I., Brown, M.G., Beron-Vera, F.J., Koçak, H., Brand, L.E., Halliwel, G.R., Shay, L.K., 2006. Persistent transport barrier on the West Florida shelf. *Geophysical Research Letters* 33, L22603. doi:10.1029/2006GL027800.
- Sanders, T.M., Garvine, R.W., 2001. Fresh water delivery to the continental shelf and subsequent mixing: an observational study. *Journal of Geophysical Research* 106 (C11), 27087–27101.
- Shaji, C., Wang, C., Halliwel, G.R., Walcraft, A., 2005. Simulation of tropical Pacific and Atlantic Oceans using a HYbrid Coordinate Ocean Model. *Ocean Modelling* 9, 253–282.
- Soares, I. D., Kourafalou, V.H., Lee, T.N., 2007a. Circulation on the eastern South Atlantic continental shelf Part I. Numerical process studies on buoyancy. *Journal of Geophysical Research* 112, C04002. doi:10.1029/2006JC003618.
- Soares, I.D., Kourafalou, V.H., Lee, T.N., 2007b. The Western South Atlantic Continental Shelf circulation. Part II: Spring and Autumn realistic simulations. *Journal of Geophysical Research* 112, C04003. doi:10.1029/2006JC003620.
- Stern, M.E., Whitehead, J.A., Hua, B.L., 1982. The intrusion of a density current along the coast of a rotation fluid. *Journal of Fluid Mechanics* 123, 237–265.
- Valle-Levinson, A., Klinck, J.M., Wheless, G.H., 1996. Inflows/outflows at the transition between a coastal plain estuary and the coastal ocean. *Continental Shelf Research* 16 (14), 1819–1847.
- Valle-Levinson, A., Holderied, K., Li, C., Chant, R.J., 2007. Subtidal flow structure at the turning region of a wide outflow plume. *Journal of Geophysical Research* 112, C04004. doi:10.1029/2006JC003746.
- Whitehead, J.A., Chapman, D.C., 1986. Laboratory observations of a gravity current on a sloping bottom: the generation of shelf waves. *Journal of Fluid Mechanics* 172, 373–399.
- Winther, N.G., Evensen, G., 2006. A hybrid coordinate ocean model for shelf sea simulation. *Ocean Modelling* 13, 221–237.
- Yankovsky, A.E., Chapman, D.C., 1997. A simple theory for the fate of buoyant coastal discharges. *Journal of Physical Oceanography* 27, 1386–1401.
- Yankovsky, A.E., 2000. The cyclonic turning and propagation of buoyant coastal discharge along the shelf. *Journal of Marine Research* 58, 585–607.
- Zalesak, S., 1979. Fully multidimensional flux-corrected transport algorithms for fluids. *Journal of Computational Physics* 31, 335–362.
- Zamudio, L., Hogan, P.J., 2008. Nesting the Gulf of Mexico in Atlantic HYCOM: oceanographic processes generated by Hurricane Ivan. *Ocean Modelling* 21, 106–125.
- Zavatarelli, M., Pinardi, N., Kourafalou, V.H., Maggiore, A., 2002. Diagnostic and prognostic model studies of the Adriatic Sea general circulation. Part 1: the seasonal variability and the role of the forcing functions. *Journal of Geophysical Research* 107(C1), 4/1–4/20.